DESY 94–152
August 1994

ISSN 0418 – 9833

On the Subtleties of Arithmetical Quantum Chaos [1]

by

R. Aurich, F. Scheffler and F. Steiner

II.Institut für Theoretische Physik , Universität Hamburg
Luruper Chaussee 149 , 22761 Hamburg
Federal Republic of Germany

Abstract

The spectral statistics of two closely related strongly chaotic quantum billiards are studied. Both are defined on the same triangular domain on the hyperbolic plane and differ only in the choice of the boundary conditions on the edges of the billiards. The fundamental domain is generated by the action of the reflection group $T^*(2,3,8)$, which is an arithmetical group leading to an exponentially degenerate length spectrum of the classical periodic orbits. The boundary conditions on one billiard, called billiard $\mathcal{A}$, are chosen such that it does not belong to a representation of the reflection group, whereas for billiard $\mathcal{B}$ the boundary conditions correspond to an irreducible symmetry representation. The crucial property of arithmetical chaos, i. e., the exponential degeneracy of periodic orbits having the same length, is not affected by the choice of the boundary conditions. For both billiards our analysis of the spectral statistics is based on the first 1050 quantal energy levels which we have computed using the boundary element method. It is found that the quantal level statistics for billiard $\mathcal{B}$ show the peculiar properties typical for arithmetical quantum chaos as discovered previously for other arithmetical systems. Billiard $\mathcal{A}$, however, behaves generically in that it shows at short– and medium–range correlations a behaviour in agreement with random–matrix theory. The periodic–orbit theory is scrutinized to shed some light on the mysterious differences between these two almost identical quantum billiards. The trace of the cosine–modulated heat kernel and the spectral form factor are studied. It is demonstrated that subtle properties of the characters attached to the classical periodic orbits are a very important ingredient in the phenomenon of arithmetical quantum chaos.

[1]Supported by Deutsche Forschungsgemeinschaft under Contract No. DFG–Ste 241/4–6

I Introduction

This paper is devoted to a study of the energy level statistics of quantum systems whose classical counterparts are strongly chaotic. Special emphasis is taken on the so–called arithmetical chaos and the peculiarities of the quantum spectrum ascribed to the exponential degeneracy of the length spectrum of the periodic orbits of the classical counterpart.

General wisdom holds that the statistical properties of quantum levels of chaotic systems are in accordance with random–matrix theory [1]. Lacking any analytical proof that random–matrix theory is applicable to quantum chaotic systems, one is doomed to carry out numerical studies. Up to now only the periodic–orbit theory [2] provides an access to a satisfactory description of the energy spectra. The predictions of random–matrix theory were first tested for the Sinai billiard [3] and the stadium billiard [4], where the level spacing statistic $P(s)$ and the spectral rigidity $\Delta_3(L)$ have been studied. Meanwhile there are many chaotic systems for which the energy spectra have been computed and compared with the predictions of random–matrix theory [2]. However, the investigations are in most cases restricted to the short– and medium–range correlations in the energy spectra which seem to confirm the agreement with random–matrix theory. The long–range correlations do not show a universal behaviour, since they are determined by the short periodic orbits which depend sensitively on the given system. According to a model [5] based on the periodic–orbit theory, the short–range correlations, in contrast, are determined by the long periodic orbits whose lengths show no sensitive dependence on the given system since they are lying exponentially dense near each other. The mean difference between neighbouring lengths is determined by the exponential proliferation of the number $N(l)$ of periodic orbits with lengths shorter than l, which is asymptotically given by $N(l) \sim \frac{e^{\tau l}}{\tau l}$, $l \to \infty$, τ being the topological entropy. The exponentially dense lying periodic orbits then blur the individual properties of a given system.

Thus the applicability of random–matrix theory to quantum chaotic systems has to be restricted to the short– and medium–range correlations which is probed by the level spacing $P(s)$ or the number variance $\Sigma^2(L)$ and the spectral rigidity $\Delta_3(L)$ for small values of L. For large L–values, the individual properties are measured. This is valid for quantum systems which do not belong to the class of *arithmetical* quantum chaotic systems. In the latter class not even the short–range correlations are in accordance with random–matrix theory, apart from the limit $L \to 0$ which is universal for both chaotic and integrable systems.

The first arithmetical quantum chaotic system for which the deviation from the random–matrix theory expectation was observed was a *triangular billiard* with Dirichlet boundary conditions which tessellates the hyperbolic plane [6]. It is denoted by $\mathrm{T}^\star(2,3,8)$ because it is characterized by the three angles $\frac{\pi}{2}, \frac{\pi}{3}$ and $\frac{\pi}{8}$ (see figure 1). The $\star$ denotes that the triangle group is actually a reflection group, which needs the complex conjugation in its representation on the Poincaré–disc. However, in the first studies the arithmetical property was not acknowledged, and the peculiar behaviour was accused to the fact that this billiard tessellates the whole hyperbolic plane. Later studies demonstrated [7] that the energy spectra of non–arithmetical (asymmetric) hyperbolic octagons, which also tessellate the hyperbolic plane, behave in accordance with random–matrix theory with respect to short– and medium–range correlations. This proved that the tessellation argument was not justified.

One was led to the special triangular billiard $\mathrm{T}^\star(2,3,8)$ by the study of the geodesic flow on compact Riemann surfaces, represented on the hyperbolic plane, which is considered as the prototype example of a strongly chaotic system. A special Riemann surface of genus $g = 2$, the so–called *regular octagon* [8], was investigated, but because of its high symmetry it has to be

desymmetrized. One of its 96 irreducible symmetry representations corresponds to this special triangular billiard.

The central characteristic of arithmetical chaotic systems was discovered at first [9] in the case of the regular octagon for which the length spectrum of periodic orbits was found to be exponentially degenerate with increasing length l according to the mean behaviour $\langle\, g(l)\,\rangle \sim \rho\frac{e^{l/2}}{l}$, $l \to \infty$, with $\rho = 8\sqrt{2}$ [9]. This exponential degeneracy of the lengths of periodic orbits was rigorously proven for the regular octagon in [10] and for general arithmetical systems in [11, 12]. A further arithmetical billiard, which played an important role in the understanding of the behaviour of arithmetical quantum systems, is Artin's billiard $\mathrm{T}^*(2,3,\infty)$ [13, 14, 15, 16].

In this paper we study the spectral statistics of two triangular quantum billiards, called $\mathcal{A}$ and $\mathcal{B}$, defined on the above mentioned hyperbolic triangle generated by the action of the reflection group $\mathrm{T}^*(2,3,8)$. The two quantum billiards differ only in the choice of the boundary conditions on the edges of the triangle. The boundary conditions for billiard $\mathcal{A}$ are chosen such that it does not belong to a representation of the reflection group, whereas for billiard $\mathcal{B}$ the boundary conditions correspond to an irreducible symmetry representation. The crucial properties of arithmetical chaos, i. e., the exponential degeneracy of the classical periodic orbits having the same length, is not affected by the choice of the boundary conditions. For both billiards our analysis is based on the first 1050 energy levels which we have computed using the boundary element method. It is found that the quantal level statistics for billiard $\mathcal{B}$ show as expected the peculiar properties typical for arithmetical quantum chaos as discovered previously in other arithmetical systems. Billiard $\mathcal{A}$, however, behaves like a generic quantum chaotic system in that it shows in the short– and medium–range correlations a behaviour in agreement with random–matrix theory. The periodic–orbit theory is scrutinized to shed some light on the mysterious differences between these almost identical quantum billiards.

In the next section we describe in more detail the two quantum billiards $\mathcal{A}$ and $\mathcal{B}$. Section III discusses the statistical properties of the quantal energy spectra with special emphasis on the differences between arithmetical and generic chaos. In section IV the periodic–orbit theory is employed to extract information about the periodic orbits from the quantal energies using the trace of the cosine–modulated heat kernel and the spectral form factor. It is demonstrated that subtle properties of the characters attached to the classical periodic orbits are a very important ingredient in the phenomenon of arithmetical quantum chaos. Section V gives a summary and discussion of the results.

II The Triangular Quantum Billiards $\mathcal{A}$ and $\mathcal{B}$

In this section we shall describe in more detail the two triangular quantum billiards $\mathcal{A}$ and $\mathcal{B}$ which are considered in this paper. Their fundamental domains are classically identical to that of the previously studied billiard $\mathrm{T}^*(2,3,8)$ with Dirichlet boundary conditions. They differ from that triangle only in the chosen boundary conditions. Instead of pure Dirichlet boundary conditions a mixture of Dirichlet and Neumann boundary conditions is imposed. The classical dynamics is not affected by the chosen boundary conditions, i. e., the classical length spectra of periodic orbits are in all cases identical with respect to the lengths and the degeneracies of the lengths. From the point of view of periodic–orbit theory the boundary conditions are only reflected by phase factors (characters) in the amplitudes of the periodic–orbit contributions. Choosing on the three sides all possible combinations of Dirichlet and Neumann boundary conditions, yields eight different quantum systems. In [17] all eight possible boundary combinations were studied. Based on the first 200 eigenvalues computed by the finite–element

method, the energy statistics were shown to be not identical for the eight systems. Four of the eight spectra behaved in accordance with random–matrix theory with respect to short– and medium–range correlations, whereas the other four showed the peculiar behaviour typical for arithmetical quantum chaotic systems. It is important to emphasize that all eight billiards possess the same length spectrum, i. e., the lengths as well as the degeneracies are identical. Thus the peculiarities must be due to a much more subtle origin than due to the degeneracies of the lengths.

Let us now discuss the billiards in more detail. They are conservative Hamiltonian systems with two degrees of freedom which classically consist of a point particle sliding freely inside a compact hyperbolic triangle $\mathcal{T}$ with elastic reflections on the boundary $\partial\mathcal{T}$. The Poincaré disc $\mathcal{D}$ is chosen as a model of the hyperbolic surface, which consists of the interior of the unit circle in the complex z–plane ($z = x_1 + ix_2$) endowed with the hyperbolic metric

$$g_{ij} \;=\; \frac{4}{(1-x_1^2-x_2^2)^2}\delta_{ij} \quad , \quad i,j = 1,2 \tag{1}$$

corresponding to constant negative Gaussian curvature $K = -1$. This fixes the length scale.

The classical motion (geodesic flow) is determined by the Hamiltonian $H = \frac{1}{2m}p_i g^{ij} p_j$, $p_i = m\, g_{ij}\, dx^j/dt$. The classical trajectories consist of geodesic pieces where the geodesics are circles intersecting the boundary of the Poincaré disc $\mathcal{D}$ perpendicularly.

The quantum mechanical system is governed by the Schrödinger equation ($z \in \mathcal{T}$)

$$-\Delta\Psi_n(z) = E_n\Psi_n(z) \quad , \quad \Delta = \frac{1}{4}(1-x_1^2-x_2^2)^2\left(\frac{\partial^2}{\partial x_1^2}+\frac{\partial^2}{\partial x_2^2}\right) \quad , \tag{2}$$

where Δ denotes the non–euclidean Laplacian corresponding to the hyperbolic metric (1). Here and in the following units $\hbar = 2m = 1$ are used. The wave functions $\Psi_n(z)$ have to obey proper boundary conditions on the boundary $\partial\mathcal{T}$ of the triangular billiard $\mathcal{T}$.

The hyperbolic triangle $\mathcal{T}$ is defined by the three angles $\alpha = \frac{\pi}{3}$, $\beta = \frac{\pi}{8}$ and $\gamma = \frac{\pi}{2}$ (see figure 1). Since the length scale is fixed ($K = -1$), the hyperbolic length a of side a is given by

$$\cosh a \;=\; \frac{\cos\alpha + \cos\beta\cos\gamma}{\sin\beta\sin\gamma} \tag{3}$$

and analogous equations for the sides b and c. One has $a = 0.764285\ldots$, $b = 0.363519\ldots$ and $c = 0.860706\ldots$. The area is given by $\mathrm{Area}(\mathcal{T}) = \pi/24$.

The triangular billiard tessellates the Poincaré disc $\mathcal{D}$ by the action of the reflection group $\mathrm{T}^*(2,3,8)$ which is generated by the three reflections along the three sides of the triangle. A close inspection of the action of the reflection group on the triangle reveals that sides b and c are mapped onto copies of each other whereas side a is only mapped onto copies of itself. The consequence is that only those combinations of boundary conditions having the same boundary condition along sides b and c are compatible with the reflection group, i. e., they correspond to a representation of the reflection group, whereas the choice of the boundary condition on side a is not restricted. Thus four combinations are obtained which belong to a representation of the reflection group, and four which do not, but all the eight classical systems nevertheless tessellate the whole Poincaré disc $\mathcal{D}$. It has been pointed out in [17] that the four triangular billiards, which yield subspectra of the spectrum of the regular octagon and are thus compatible with the reflection group, show the peculiar behaviour characteristic for arithmetical chaos, while the other four behave according to random–matrix theory at small– and medium–range correlations.

It is worthwhile to note that Gutzwiller's semiclassical periodic–orbit theory [2] is only exact for the compatible case, since only in that case one can derive the trace formula without any approximation as Selberg has shown for general Fuchsian groups [18].

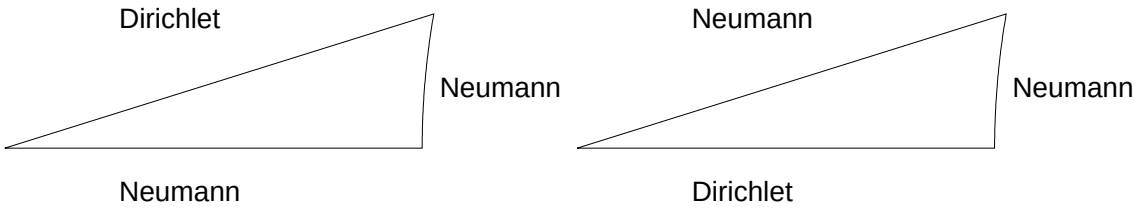

Figure 1: The quantum billiards $\mathcal{A}$ and $\mathcal{B}$ in the Poincaré disc $\mathcal{D}$. The left triangle defines billiard $\mathcal{A}$ with Neumann boundary conditions on sides a and b, and Dirichlet boundary condition on side c. The right triangle shows billiard $\mathcal{B}$ with Dirichlet boundary condition on side a, and Neumann boundary conditions on sides b and c. The left corners of the triangles are at the origin $z = 0$ of the Poincaré disc $\mathcal{D}$ whose boundary $|z| = 1$ is not shown.

We choose the following two combinations of boundary conditions: For the incompatible case we choose Neumann boundary conditions on sides a and b and Dirichlet boundary condition on side c. In the following this quantum billiard is called billiard $\mathcal{A}$. The other billiard, which we call billiard $\mathcal{B}$, is defined by a Dirichlet condition on side a and Neumann conditions on sides b and c. The quantum billiard $\mathcal{B}$ represents the compatible case which corresponds to a representation of the reflection group. Both billiards are illustrated in figure 1. We would like to emphasize that billiard $\mathcal{A}$ as well as billiard $\mathcal{B}$ possess the same arithmetical structure leading to the same length spectrum of periodic orbits. Using the boundary element method [19] we have computed all quantal energies $0 < E_1 \leq E_2 \leq \ldots$ up to $E = 100\,000$ containing roughly 1050 levels for each billiard. The ground–state energies are $E_1 = 45.58$ for billiard $\mathcal{A}$, and $E_1 = 32.67$ for billiard $\mathcal{B}$. We observe no degeneracies among the computed quantal levels.

III Level Statistics

III.1 The Weyl Series

The first step in the analysis of the statistical properties of the quantal levels of billiard $\mathcal{A}$ and billiard $\mathcal{B}$, respectively, is the unfolding of their energy spectra. The quantal energies E_n are mapped by

$$x_n \;=\; \overline{\mathcal{N}}(E_n) \tag{4}$$

onto a normalized spectrum $\{x_n\}$ having a mean level spacing of unity. Here $\overline{\mathcal{N}}(E)$ denotes the Weyl series which describes the asymptotic behaviour of the spectral staircase $\mathcal{N}(E)$ counting the quantal levels up to energy E

$$\overline{\mathcal{N}}(E) \;=\; \frac{\mathrm{Area}(\mathcal{T})}{4\pi}\, E \;+\; \frac{\varepsilon^a a + \varepsilon^b b + \varepsilon^c c}{4\pi}\,\sqrt{E} \;+\; \sigma \quad , \tag{5}$$

where $\mathrm{Area}(\mathcal{T}) = \pi/24$ denotes the area of the triangle, and a, b and c are the hyperbolic lengths of the corresponding sides (see eq.(3)). The boundary conditions determine ε^i to be

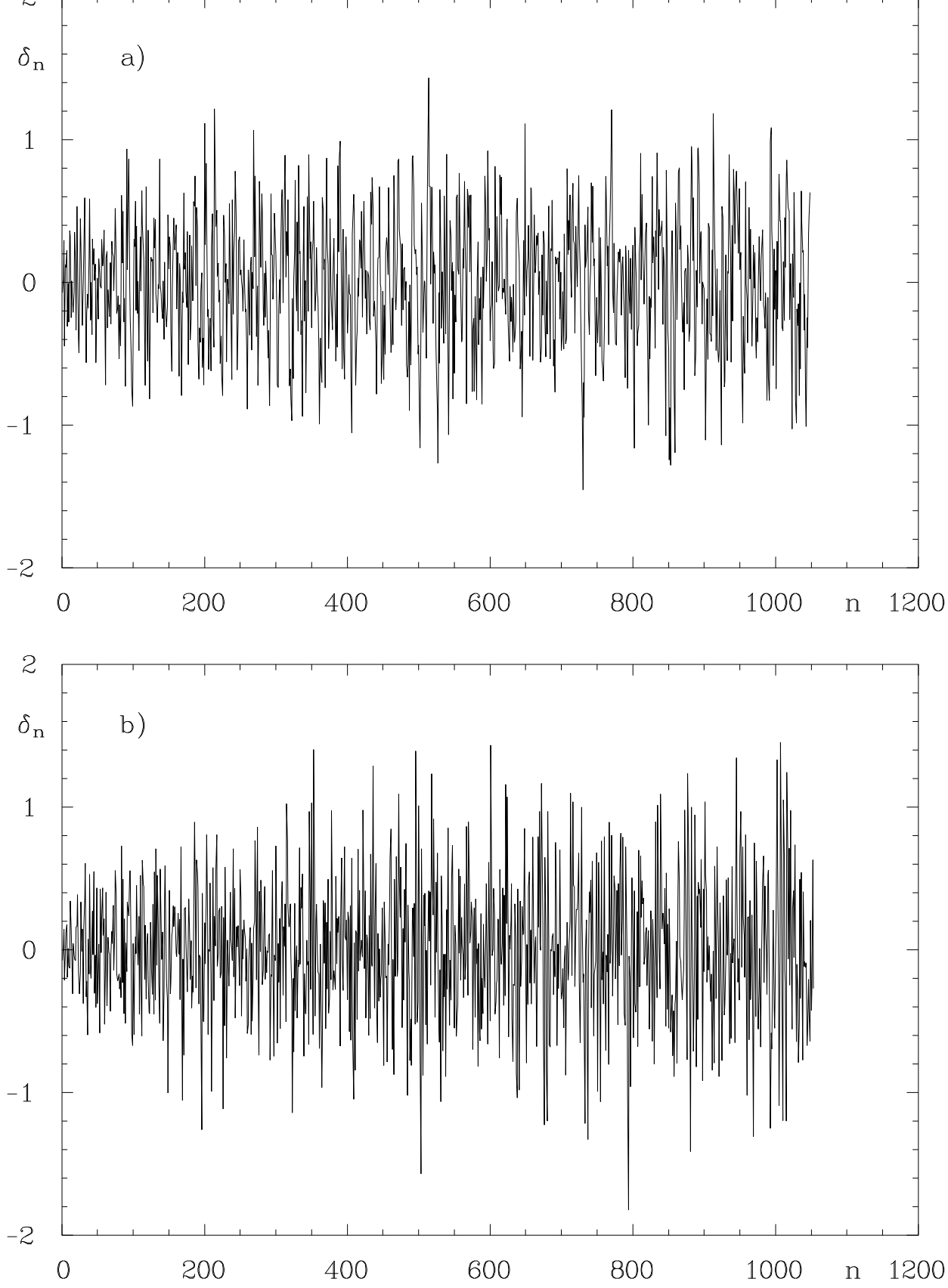

Figure 2: The spectral fluctuations δ_n are shown for billiard $\mathcal{A}$ in a) and for billiard $\mathcal{B}$ in b).

$+1$ for a Neumann boundary condition and -1 for a Dirichlet condition. The constant σ is obtained from a fit to the energy spectra yielding -0.188 for billiard $\mathcal{A}$, and -0.125 for billiard $\mathcal{B}$. (See also the discussion at the end of Sec. IV.1.) In figure 2 the spectral fluctuations

$$\delta_n := x_n - (n - \frac{1}{2}) \quad , \quad n = 1, 2, 3, \ldots \tag{6}$$

are plotted for both billiards. In both cases one observes fluctuations around zero which illustrates that the Weyl series (5) describes indeed the mean behaviour of the smoothed counting function $\mathcal{N}(E)$. In addition, this shows, that there are no missing levels in the computed spectra.

III.2 The Level Spacing Statistic $P(s)$

One of the simplest statistics is the level spacing statistic $P(s)$ which describes the distribution of the spacings $s_n = x_{n+1} - x_n$ of adjacent quantal levels. Since the billiards are invariant under time reversal, one has to compare the energy statistics with the Gaussian orthogonal ensemble (GOE) of random matrix theory [1]. The GOE level spacing is well approximated by Wigner's surmise

$$P_{\mathrm{GOE}}(s) \simeq \frac{\pi}{2} s e^{-\frac{\pi}{4}s^2} \tag{7}$$

showing a linear level repulsion for $s \to 0$ which is typical for quantum chaotic systems with time reversal symmetry. In contrast, integrable systems are expected to possess Poisson distributed quantal levels whose level spacing is given by

$$P_{\mathrm{Poisson}}(s) = e^{-s} \tag{8}$$

which is maximal for $s = 0$ and thus shows level attraction in striking contrast to the GOE case. The level spacings $P(s)$ are displayed in figure 3. The level spacing for billiard $\mathcal{A}$ containing all levels up to $E = 100\,000$ is shown in figure 3a in comparison with Wigner's surmise (7), and very good agreement is observed. Figure 3b shows $P(s)$ for billiard $\mathcal{B}$, again using all levels up to $E = 100\,000$ in comparison with the Poisson level spacing (8). In this case the level spacing does not reveal any indication of level repulsion and violates clearly the GOE behaviour. It is impressive to see the striking difference between the two cases since only a slight alteration of the boundary conditions, i. e., the interchange of the boundary conditions on sides a and c, distinguishes these otherwise identical billiards. But notice that billiard $\mathcal{B}$ does not show agreement with the Poisson expectation. Nevertheless, it may be that the Poisson behaviour is reached in the semiclassical limit $E \to \infty$. This is indeed the case for Artin's billiard, another arithmetical billiard, for which $P(s)$ has been computed in two energy ranges in [14]. There it is observed that $P(s)$ approaches in the low–energy range at $s = 0$ a value of roughly 0.6 similar to our case. In addition, in [14] $P(s)$ is shown for a very high energy range where good agreement with the Poisson curve is observed. To test the possibility that billiard $\mathcal{B}$ behaves in an analogous way, we split the energy interval into $E \in [0, 50\,000]$ and into $E \in [50\,000, 100\,000]$. The result is shown in figures 3c and 3d. The distribution indeed tends at higher energies more to the Poisson curve, and at $s = 0$ the distribution increases roughly from 0.4 to 0.7. The numerical results thus may be interpreted to indicate that the level spacing of billiard $\mathcal{B}$ approaches a Poisson distribution in the semiclassical limit. If this would indeed be the case there arises the interesting question why the semiclassical limit is reached so slowly in comparison to billiard $\mathcal{A}$, for which the GOE curve is already a satisfactory description in the

low–energy range, a fact which has often been observed for other systems, and, as an example, we would like to recall the results in the case of the asymmetric hyperbolic octagons [7] where the energy statistics were studied for an ensemble of 30 different octagons. A superposition of their spectra with only the first 75 quantal level shows already a striking agreement with the GOE prediction.

Since the level spacing statistics of arithmetical chaotic systems are not stationary in the commonly accessible energy range comprising the first one–thousand levels a further property has been found which distinguishes arithmetical systems from the generic class.

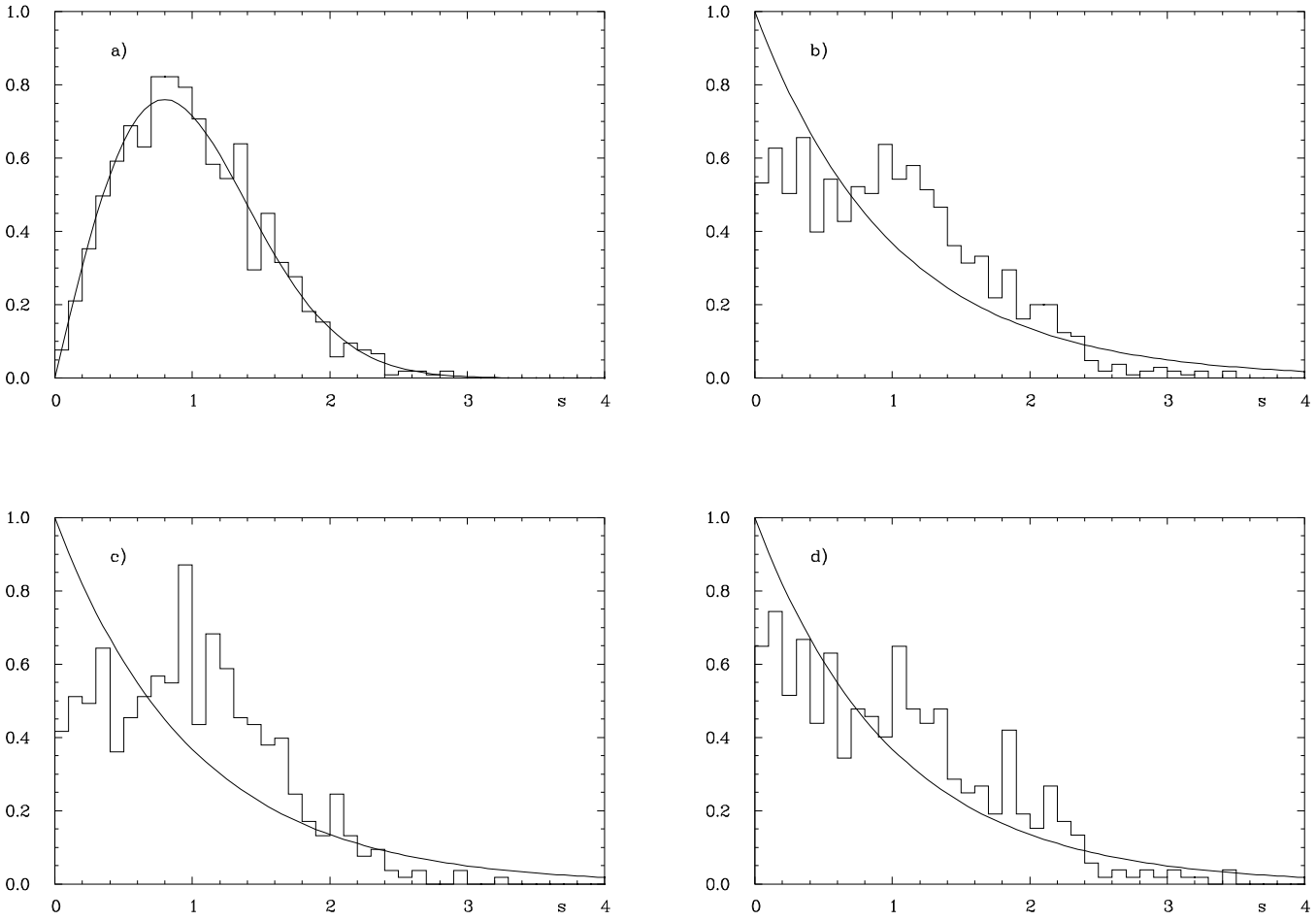

Figure 3: The level spacing $P(s)$ is displayed for billiard $\mathcal{A}$ in comparison with Wigner's surmise (7) in figure a) for all energies $E_n < 100\,000$. Figures b) to d) show $P(s)$ for billiard $\mathcal{B}$ for the energy ranges b) $E_n \in [0, 100\,000]$, c) $E_n \in [0, 50\,000]$, and d) $E_n \in [50\,000, 100\,000]$. The smooth curve in figures b) to d) represents the Poisson expectation (8).

III.3 The Number Variance $\Sigma^2(L)$

The number variance allows a convenient inspection of the properties of the energy spectrum over all scales of correlation lengths. In contrast to the nearest neighbour level spacing $P(s)$, which measures only short correlation lengths, the number variance $\Sigma^2(L)$ probes the spectrum over all correlation lengths L. The number variance describes the fluctuations of the number

$n(L)$ of levels contained in a randomly chosen interval of length L and is defined as

$$\Sigma^2(L) \;:=\; \Big\langle\, (n(L)-L)^2 \,\Big\rangle \quad , \tag{9}$$

where the brackets $\langle \ldots \rangle$ denote a local averaging over sufficiently many levels. In definition (9) it is assumed that the energy spectrum is already unfolded such that $\langle\, n(L) \,\rangle \;=\; L$. For GOE matrices the random–matrix theory yields for the number variance the following exact result

$$\Sigma^2_{\rm GOE}(L) \;=\; \frac{2}{\pi^2}\,\Big\{\, \ln(2\pi L)+\gamma+1+\frac{1}{2}{\rm Si}^2(\pi L)-\frac{\pi}{2}{\rm Si}(\pi L)-\cos(2\pi L) \\ -{\rm Ci}(2\pi L)+\pi^2 L\left(1-\frac{2}{\pi}{\rm Si}(2\pi L)\right)\Big\} \quad , \tag{10}$$

where γ denotes Euler's constant. Many quantum chaotic systems show a reasonably good agreement with (10) for short– and medium–range correlations. In the large L–range they typically display a fluctuating behaviour around a plateau, whereas in the GOE case the number variance $\Sigma^2_{\rm GOE}(L)$ increases logarithmically for $L \to \infty$ as determined by the first term in (10).

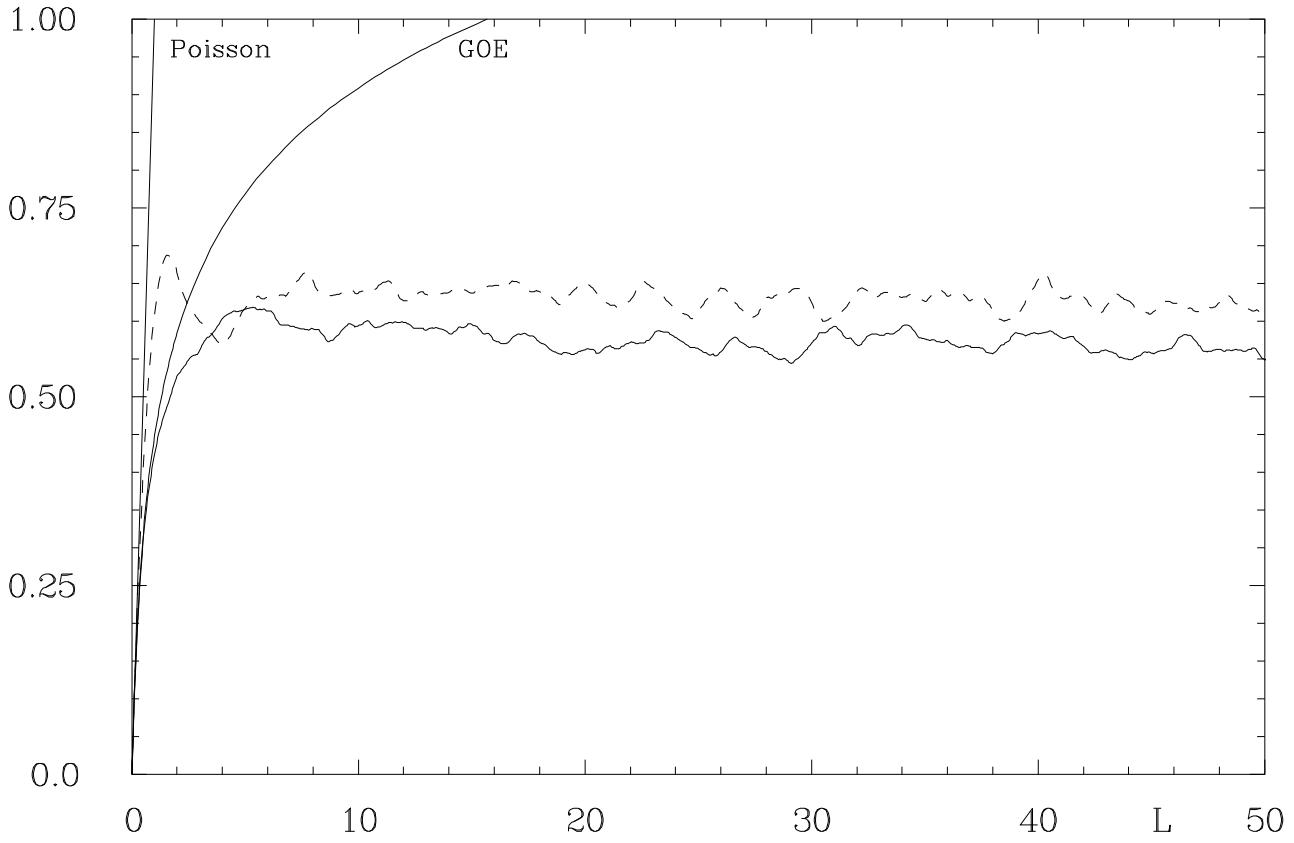

Figure 4: The number variance $\Sigma^2(L)$ is presented for billiard $\mathcal{A}$ (full curve) and for billiard $\mathcal{B}$ (dashed curve) in comparison with the GOE expectation (10) and the Poisson expectation. All quantal levels up to $E = 100\,000$ have been used.

Let us now discuss the number variance for the two billiards. We choose a rectangular averaging for the local average $\langle \ldots \rangle$. In figure 4 the number variance is shown for billiard $\mathcal{A}$ (full curve) and for billiard $\mathcal{B}$ (dashed curve) in comparison with the GOE expectation and the Poisson behaviour given by $\Sigma^2_{\rm Poisson}(L) = L$. In this evaluation all quantal levels up to

$E = 100\,000$ have been used. One observes that billiard $\mathcal{A}$, which already displayed for the level spacing a generic behaviour, is in good agreement with the GOE behaviour up to roughly $L \simeq 1 \ldots 2$ and fluctuates thereafter around its saturation plateau

$$\Sigma^2_\infty := \lim_{L\to\infty} \left\langle \Sigma^2(L) \right\rangle_L \quad , \tag{11}$$

where $\langle \ldots \rangle_L$ denotes an averaging over a sufficiently large L–interval. Thus there is only a very small L–interval corresponding to short–range correlations where the GOE prediction agrees with the number variance. This small interval of agreement between $\Sigma^2(L)$ and the GOE behaviour is responsible for the observed GOE–like nearest–neighbour level spacing $P(s)$ which measures essentially the range $L < 2$. This small range is also the range in which a different behaviour is revealed by billiard $\mathcal{B}$ which matches there much better a Poisson behaviour. Up to $L \simeq 2$ the number variance of billiard $\mathcal{B}$ lies well above the GOE curve. For larger L–values there are again the characteristic fluctuations around a plateau. Thus both billiards show a different behaviour only for the short–range correlations, while the medium– and long–range correlations are very similar in both cases. If one studies only the nearest–neighbour level spacings one might be misled to the conclusion that billiard $\mathcal{A}$ shows GOE behaviour and billiard $\mathcal{B}$ Poisson behaviour. However, this is only true for $L < 2$.

In figure 5 the number variance is shown for four distinct energy ranges. The energy dependence of the saturation plateau Σ^2_∞ is clearly visible. The available energy range has been split in four intervals of length $\Delta E = 25\,000$, i. e., $E \in [0, 25\,000]$ (full curve), $E \in [25\,000, 50\,000]$ (dotted curve), $E \in [50\,000, 75\,000]$ (dashed curve), and $E \in [75\,000, 100\,000]$ (dashed–dotted curve). Figure 5a displays the results for billiard $\mathcal{A}$, and figure 5b for billiard $\mathcal{B}$. In most cases the saturation plateau Σ^2_∞ increases with energy. However, in figure 5a the dotted curve belonging to the energy range $E \in [25\,000, 50\,000]$ lies mostly above the dashed curve corresponding to $E \in [50\,000, 75\,000]$. The general tendency is nevertheless an increasing plateau with increasing energy. One observes again a similar behaviour for the two billiards except for the small L–range, $L < 2$, where the GOE curve is a reasonably good description for billiard $\mathcal{A}$ and the Poisson curve for billiard $\mathcal{B}$. In addition the range of agreement increases with increasing energy in general.

III.4 The Spectral Rigidity $\Delta_3(L)$

A similar statistic which has also played a major role in the study of the properties of quantal energy spectra is the spectral rigidity $\Delta_3(L)$ introduced by Dyson and Mehta [20]. The spectral rigidity is defined as the average of the mean square deviation of the staircase $\mathcal{N}(x)$ of the unfolded energy spectrum $\{x_n\} = \{\overline{\mathcal{N}}(E_n)\}$ from the best fitting straight line $a + b\varepsilon$

$$\Delta_3(L) := \left\langle \min_{(a,b)} \frac{1}{L} \int_{-L/2}^{L/2} d\varepsilon \left[\mathcal{N}(x+\varepsilon) - a - b\varepsilon\right]^2 \right\rangle \quad , \quad x := \overline{\mathcal{N}}(E) \quad , \tag{12}$$

where $\langle \ldots \rangle$ again denotes a local average. The constants a and b can be eliminated yielding the well–known expression

$$\Delta_3(L) = \left\langle \frac{1}{L}\int_{-L/2}^{L/2} d\varepsilon \mathcal{N}^2(x+\varepsilon) - \left[\frac{1}{L}\int_{-L/2}^{L/2} d\varepsilon \mathcal{N}(x+\varepsilon)\right]^2 - 12\left[\frac{1}{L^2}\int_{-L/2}^{L/2} d\varepsilon\varepsilon \mathcal{N}(x+\varepsilon)\right]^2 \right\rangle \quad . \tag{13}$$

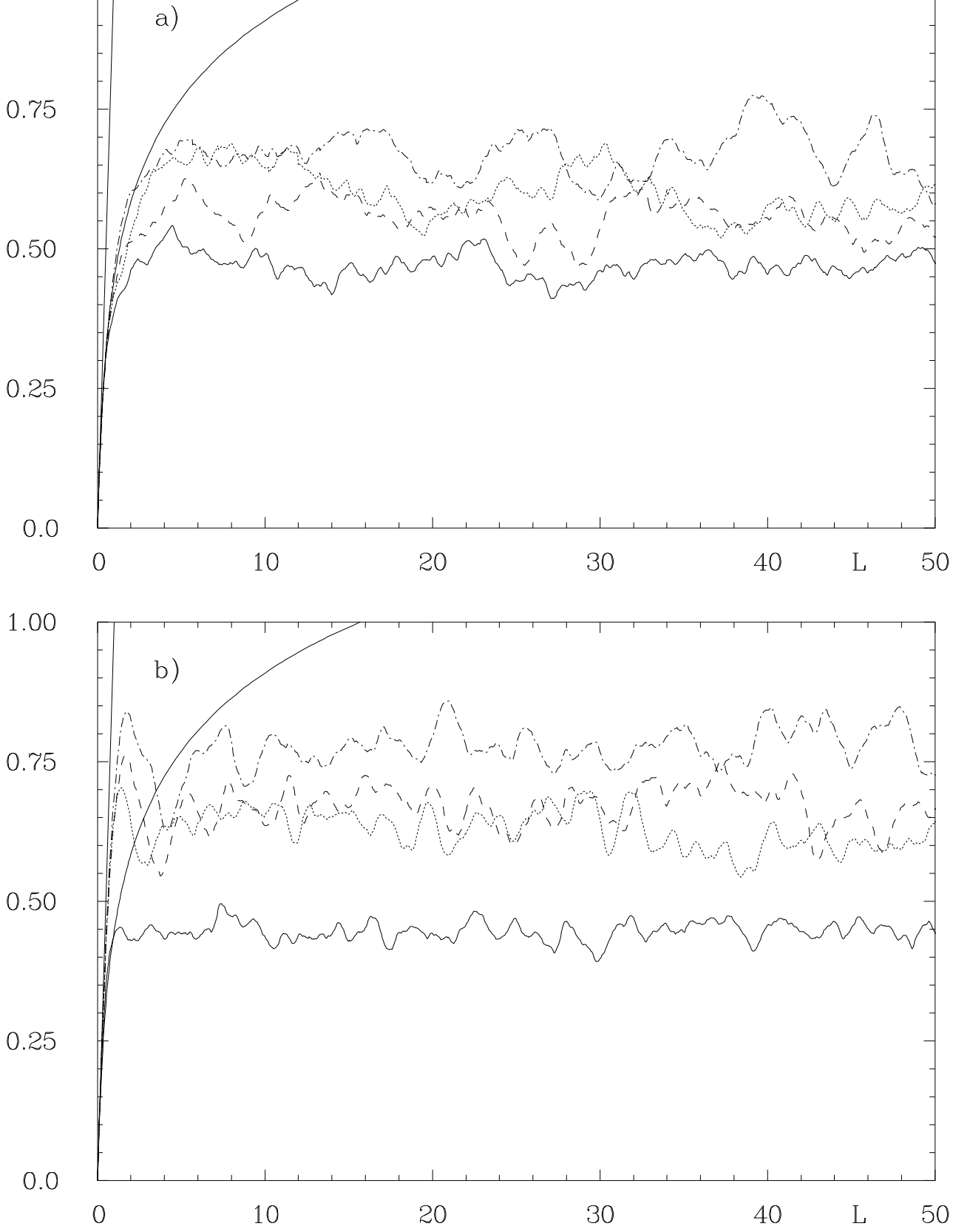

Figure 5: The energy dependence of the number variance is shown for billiard $\mathcal{A}$ in a) and for billiard $\mathcal{B}$ in b). The four curves correspond to the four energy intervals as explained in the text. In addition the Poisson and the GOE expectation are displayed.

The spectral rigidity $\Delta_3(L)$ is in the case of random matrices closely related to the number variance by the equation

$$\Delta_3^{\mathrm{RMT}}(L) \;=\; \frac{2}{L^4}\;\int_0^L\;\left(\;L^3-2L^2r+r^3\;\right)\;\Sigma^2_{\mathrm{RMT}}(r)\;dr \quad . \tag{14}$$

The GOE behaviour of the spectral rigidity is determined by equations (10) and (14). Based on Gutzwiller's periodic–orbit theory [2] Berry gives in [5] arguments why the spectral rigidity shows for energy spectra of chaotic systems a saturation for $L \gg L_{\max}$ and a behaviour consistent with random–matrix theory below $L_{\max}$, where $L_{\max} = 2\pi\overline{d}(E)/T_{\min}$ with $T_{\min}$ being the period of the shortest periodic orbit and $\overline{d}(E)$ the mean level density. Furthermore it is expected that the saturation value $\Delta_\infty := \lim_{L\to\infty}\Delta_3(L)$ increases logarithmically with increasing energy E. According to the arguments given by Berry [5], one expects for billiards $\mathcal{A}$ and $\mathcal{B}$ the following energy dependence

$$\Delta_\infty(E) \;=\; \frac{1}{2\pi^2}\,\log E \;+\; c(l_0) \quad , \tag{15}$$

where the constant is in its crudest approximation given by $c(l_0) = \frac{1}{\pi^2}\log(4\pi e\overline{d}(E)/l_0) - \frac{1}{8}$ with $l_0 = 0.6330\ldots$ being the length of the shortest periodic orbit. The mean level density $\overline{d}(E)$ is for two–dimensional billiards a constant plus non–leading terms, and for our billiards it is given by (see eq.(5)) $\overline{d}(E) = \frac{1}{96} + O(E^{-1/2})$. With these values one obtains $c(l_0) = -0.18336\ldots$. For integrable systems one expects instead the semiclassical behaviour $\Delta_\infty(E) \sim \sqrt{E}$.

In figure 6 the spectral rigidity $\Delta_3(L)$ is shown for billiard $\mathcal{A}$ (full curve) and billiard $\mathcal{B}$ (dashed curve) in comparison with the GOE and Poisson expectations using all quantal levels up to $E = 100\,000$. As in the case of the number variance, one observes at small correlation lengths $L < 4$ a reasonable agreement with the GOE curve for billiard $\mathcal{A}$ and with the Poisson curve for billiard $\mathcal{B}$. The spectral rigidity of billiard $\mathcal{B}$ lies clearly above the GOE curve for $L < 15$ so that a saturation effect cannot be claimed as the cause for the deviation from the GOE curve. The saturation behaviour is similar for both billiards except the fact that the saturation value is slightly larger for billiard $\mathcal{B}$.

Since the spectral rigidity shows a much smoother behaviour than the number variance, it is more suited for a study of the energy dependence of the saturation of the energy fluctuations. In figure 7 the spectral rigidity is shown for the same energy intervals as in figure 5, where figure 7a deals with billiard $\mathcal{A}$ and figure 7b with billiard $\mathcal{B}$. It is seen that the GOE and the Poisson behaviour is matched, respectively, over an increasing interval with increasing energy until the spectral rigidities drop below the GOE or Poisson behaviour to approach their saturation values. The saturation values again show the tendency towards higher values with increasing energy. One again observes an exception in the case of billiard $\mathcal{A}$ where the dotted curve belonging to the energy range $[25\,000, 50\,000]$ lies above the dashed curve belonging to $[50\,000, 75\,000]$.

If arithmetical quantum chaotic systems behave more like integrable systems with respect to their spectral statistics, one would expect that the saturation value goes like $\Delta_\infty(E) = \alpha\sqrt{E}+\beta$ in the case of billiard $\mathcal{B}$ and like $\Delta_\infty(E) = \frac{1}{2\pi^2}\log E + \gamma$ in the case of billiard $\mathcal{A}$. To test this hypothesis we computed the saturation values over an energy range $[E_n, E_n + \Delta E]$ with $E_n = 10\,000(n-1)$, $n = 1, 2, \ldots, 8$ and $\Delta E = 30\,000$ yielding eight intervals in the available range $[0, 100\,000]$. The saturation value Δ_∞ itself was determined from a fit of $\Delta_3(L)$ in the range $L \in [15, 50]$ to the function

$$f_\Delta(L) \;=\; \Delta_\infty\;\left(1+\frac{c_1}{L}+\frac{c_2}{L^2}\right) \quad , \tag{16}$$

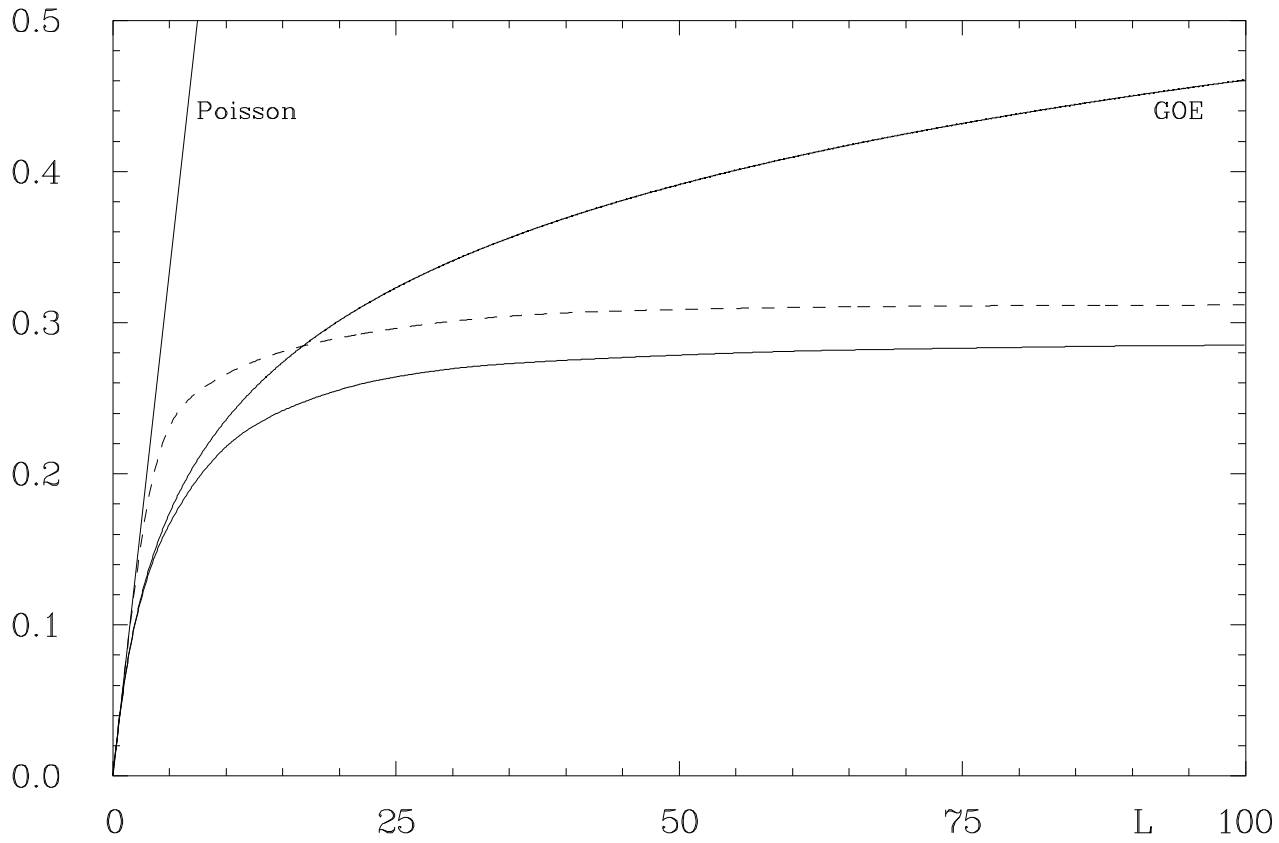

Figure 6: The spectral rigidity $\Delta_3(L)$ is presented for billiard $\mathcal{A}$ (full curve) and for billiard $\mathcal{B}$ (dashed curve) in comparison with the GOE expectation and the Poisson expectation. All quantal levels up to $E = 100\,000$ have been used.

where Δ_∞, c_1 and c_2 are the fit parameters. In this way we obtained 8 saturation values for each billiard which in turn allows a fit of $\Delta_\infty(E)$. The fit parameters obtained are $\alpha = 9.7633 \times 10^{-4}$, $\beta = 0.11569$ and $\gamma = -0.24998$. The results are shown in figure 8. The values for billiard $\mathcal{A}$ are shown as full circles in comparison with the logarithmic fit function (full curve) using the above value for γ. The fit is reasonably good. The main deviation occurs for billiard $\mathcal{A}$ at $E = 65\,000$ where the saturation value drops somewhat below the fit. It is the same anomaly we have already observed in the figures presenting the energy dependence of the number variance and the spectral rigidity. However, over the whole energy range considered the logarithmic increase is confirmed. The fit constant γ differs from the approximation $c(l_0)$ given below eq.(15) by a value of 0.06662. This may appear as a small difference, however, a look at figure 8 reveals that the constant $c(l_0)$ would yield too large saturation values.

The saturation values $\Delta_\infty(E)$ of the arithmetically behaving billiard $\mathcal{B}$ shown as circles in figure 8 are in almost perfect agreement with a "$\sqrt{E}$–behaviour" characteristic for integrable systems which is shown as the dotted curve. A logarithmic behaviour seems to be excluded. Arguments based on the diagonal approximation of the spectral form factor lead to a "$\sqrt{E}/\log E$–behaviour" [12], but since this gives an unsatisfactory description to our data, we use in the following the more appropriate "$\sqrt{E}$–behaviour". A knowledge of the energy dependence of the saturation value of the spectral rigidity is of crucial importance for the mode fluctuation distribution we would like to discuss in the next section.

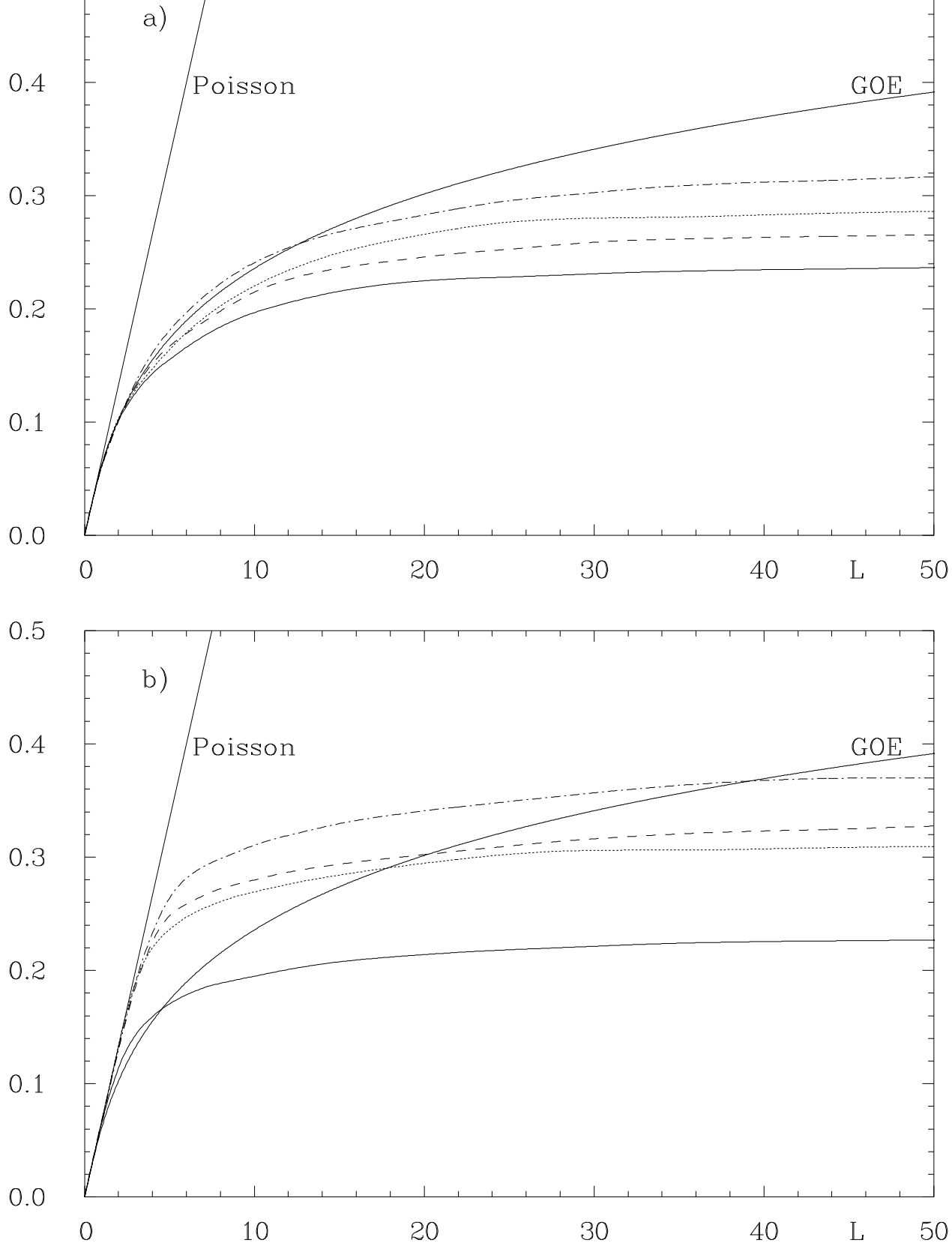

Figure 7: The energy dependence of the spectral rigidity is shown for billiard $\mathcal{A}$ in a) and for billiard $\mathcal{B}$ in b). The four curves correspond to the same four energy intervals as in figure 5. In addition the Poisson and the GOE expectation are displayed.

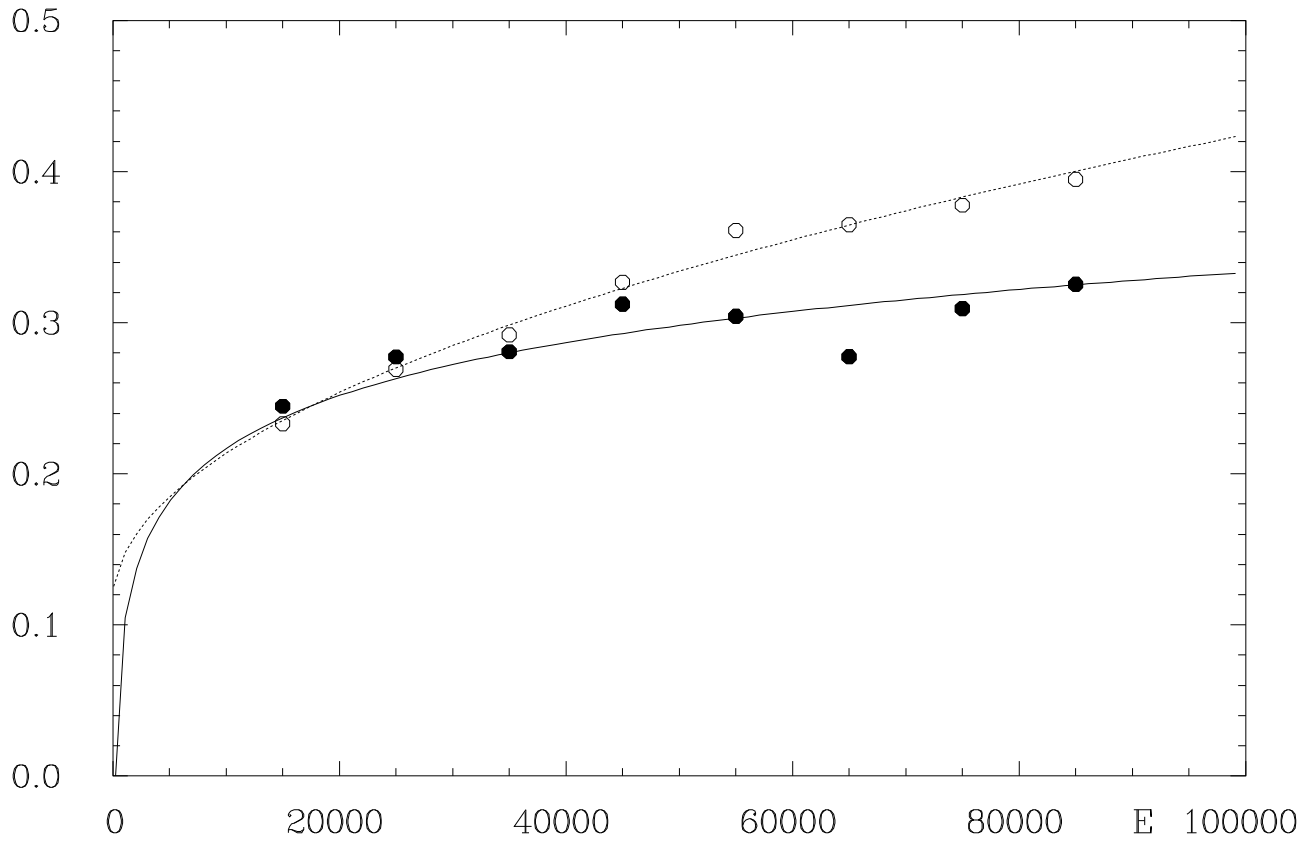

Figure 8: The energy dependence of the saturation value Δ_∞ of the spectral rigidity is shown. The full dots and the full curve, i. e., the fit result, belong to billiard $\mathcal{A}$, whereas the circles and the dotted curve belong to billiard $\mathcal{B}$.

III.5 The Mode Fluctuation Distribution $P(W)$

We have seen in the preceding sections that the hypothesis [3, 4] that quantum chaotic systems display level fluctuations according to random–matrix theory only holds at small– and medium–range correlations. Thus one has to seek for other statistical measures which are able to uncover the fingerprints of classical chaos in quantum chaotic systems. To this aim the distribution $P(W)$ of the mode fluctuation $W(E)$ has been proposed in [21, 22] as a novel quantity to measure quantum chaos. The (normalized) mode fluctuation $W(E)$ is defined by

$$W(E) \;:=\; \frac{\mathcal{N}_{\rm fl}(E)}{\sqrt{\Delta_\infty(E)}} \quad , \tag{17}$$

where $\mathcal{N}_{\rm fl}(E) := \mathcal{N}(E) - \overline{\mathcal{N}}(E)$ is the fluctuating part of the mode number $\mathcal{N}(E)$ (spectral staircase function). Since the Weyl series $\overline{\mathcal{N}}(E)$, see eq.(5), describes the mean mode number, it follows that $\mathcal{N}_{\rm fl}(E)$ fluctuates by definition around zero ($\Delta E \gg 1/\overline{d}(E)$)

$$\left\langle \frac{1}{\Delta E} \int_{E-\Delta E/2}^{E+\Delta E/2} dE'\, \mathcal{N}_{\rm fl}(E') \right\rangle \;\to\; 0 \quad , \quad E \to \infty \quad , \tag{18}$$

which in turn implies that the value distribution of $W(E)$, $P(W)$, has zero–mean. Furthermore, the second moment of $\mathcal{N}_{\rm fl}(E)$ obeys asymptotically [12]

$$\left\langle \frac{1}{\Delta E} \int_{E-\Delta E/2}^{E+\Delta E/2} dE'\, \mathcal{N}_{\rm fl}^2(E') \right\rangle \;\sim\; \Delta_\infty(E) \quad , \quad E \to \infty \quad , \tag{19}$$

and thus the division by $\sqrt{\Delta_\infty(E)}$ correctly normalizes the distribution of $W(E)$ having unit variance. Since the distribution $P(W)$ has zero mean and unit variance, its specific form is the important measure. In [21, 22] the conjecture has been put forward that classically strongly chaotic systems should display for $E \to \infty$ a universal Gaussian behaviour

$$P_{\text{Gaussian}}(W) \;=\; \frac{1}{\sqrt{2\pi}}\, e^{-\frac{1}{2}W^2} \quad , \tag{20}$$

independent of whether the system shows generic or arithmetical chaos, whereas classically integrable systems should betray themselves by a non–Gaussian distribution $P(W)$. In addition to numerical tests for three different systems, there are further theoretical arguments in support of this hypothesis which have been given in [22]. For some integrable systems, a non–Gaussian distribution has been rigorously proven [23] to hold, whereas the Gaussian is proven to be the exact limit distribution for the non–trivial zeros of the Riemann zeta function using Selberg's moment formalism [24]. The Riemann zeros are interpreted as quantal levels of an unknown quantum chaotic system without time–reversal symmetry.

It should be noted that a Gaussian distribution corresponds to maximally random spectra being in agreement with the intuitive prejudice one has on chaotic systems.

We have computed the distribution $P(W)$ for both billiards $\mathcal{A}$ and $\mathcal{B}$ using for $\Delta_\infty(E)$ in the definition (17) the corresponding fits shown in figure 8. In figure 9a the result is shown for the generically behaving billiard $\mathcal{A}$, while figure 9b presents the results for the arithmetically behaving billiard $\mathcal{B}$. The histograms are computed by evaluating $W(E)$ in steps of $\Delta E = 5$ which gives 20 000 data points up to $E = 100\,000$. The parameter–free expectation (20) is shown as a full curve. The agreement is impressive and underscores the fact that this statistic is universal in that it yields the same distribution for arithmetical and non–arithmetical quantum chaotic systems. We have also applied the Kolmogorov–Smirnov test to the cumulative mode fluctuation distribution testing the cumulative version of the prediction (20). The Kolmogorov–Smirnov test yields the approximate significance level $\mathcal{P}$ of the maximal distance between the cumulative distribution and the theoretical prediction, i. e., $\mathcal{P}$ is the probability to obtain a maximal distance greater than the observed one. For both billiards we obtained high significance levels $\mathcal{P} \gg 1\%$. We get $\mathcal{P} = 23\%$ for billiard $\mathcal{A}$, and $\mathcal{P} = 44\%$ for billiard $\mathcal{B}$. Thus the Kolmogorov–Smirnov test confirms the expectation (20).

IV Periodic–Orbit Theory

IV.1 The Trace Formula

It is most interesting to inquire the periodic–orbit theory with respect to the level statistics of billiards $\mathcal{A}$ and $\mathcal{B}$. Since both systems have the same classical periodic orbits, i. e., the same lengths and multiplicities, the differences in the level fluctuations over small– and medium–range correlations must be explained by the phase factors attached to the periodic orbits. The starting point is the Selberg trace formula [18] for such billiards. The Selberg trace formula has been specified in [8] for hyperbolic billiards with identical boundary conditions on all sides, i. e., either only Dirichlet or only Neumann boundary conditions. For the case of mixed boundary conditions compatible with a reflection group Γ, e. g. $\Gamma = \mathrm{T}^*(2,3,8)$, i. e., billiard $\mathcal{B}$ or a billiard with Neumann boundary condition on side a and Dirichlet boundary conditions on sides b and

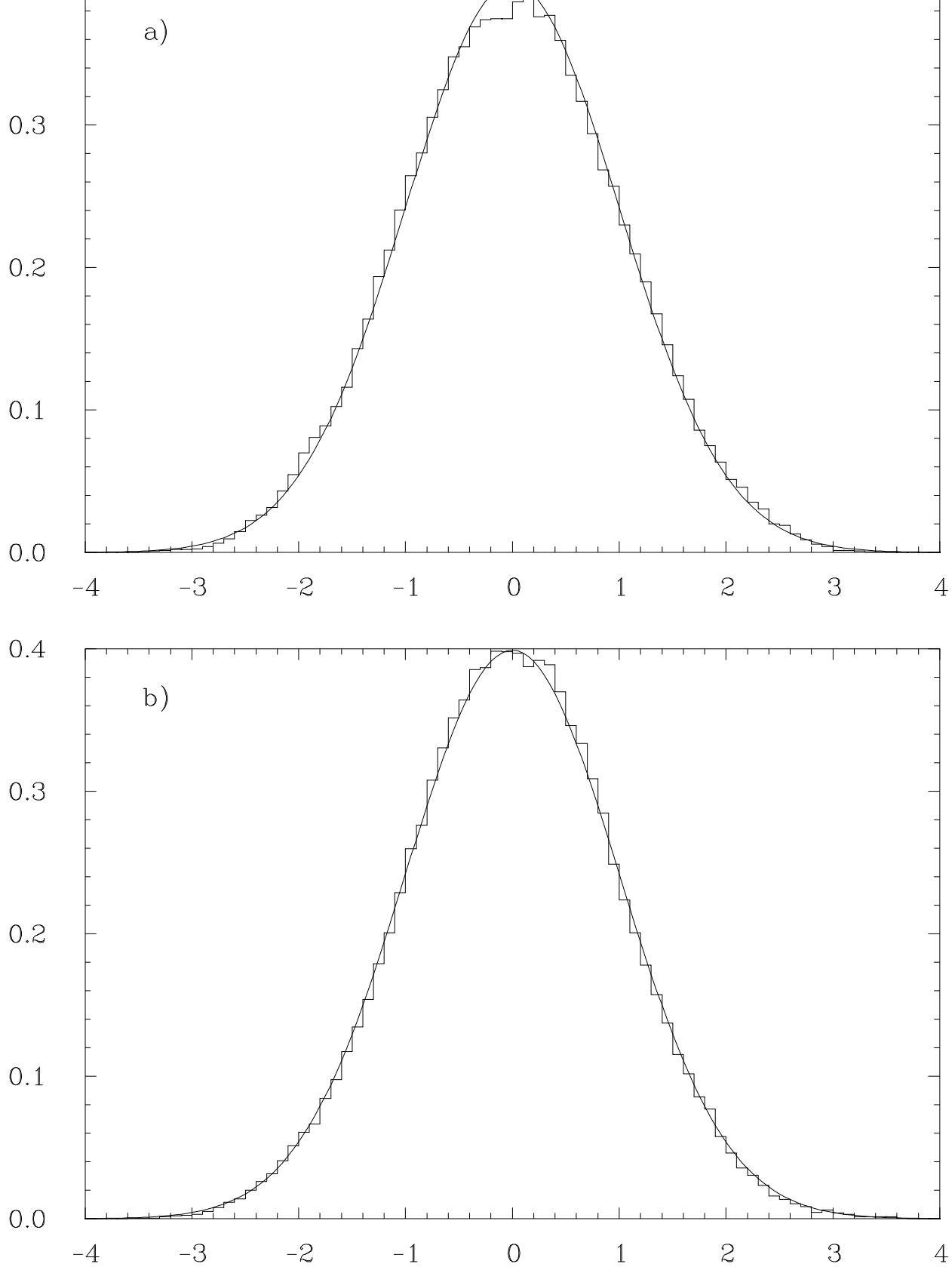

Figure 9: The mode fluctuation statistic $P(W)$ is shown for billiard $\mathcal{A}$ in figure a), and for billiard $\mathcal{B}$ in figure b) in comparison with the prediction (20) (full curve).

c, the trace formula was derived first in [25] and is given by

$$\begin{aligned}
\sum_{n=1}^{\infty} h(p_n) &= \frac{\mathrm{Area}(\mathcal{T})}{4\pi} \int_{-\infty}^{\infty} dp\; h(p)\; p\; \tanh(\pi p) \;+\; \sum_{t_{\mathrm{inv}}} \frac{\chi(t)\, l(t)}{4}\, g(0) \\
&+ \sum_{t_{\mathrm{ellip}}} \sum_{k=1}^{m_t-1} \frac{\chi^k(t)}{4m_t \sin(\frac{\pi k}{m_t})} \int_{-\infty}^{\infty} dp\; h(p)\; \frac{\exp(-2\pi p \frac{k}{m_t})}{1+\exp(-2\pi p)} \\
&+ \sum_{t_{\mathrm{sing}}} \sum_{k=1}^{\infty} \frac{l(t)}{4} \left\{ \frac{\chi^k(t_{\mathrm{even}})}{\sinh(kl(t)/2)} + \frac{\chi(t_{\mathrm{odd}})\,\chi^{k-1}(t_{\mathrm{even}})}{\cosh(kl(t)/2)} \right\} g(kl(t)) \\
&+ \sum_{t_{\mathrm{hyp}}} \sum_{k=1}^{\infty} \frac{\chi^k(t)\; l(t)}{\exp(kl(t)/2) - \sigma(t)^k \exp(-kl(t)/2)}\, g(kl(t)) \quad . \qquad (21)
\end{aligned}$$

The left–hand side of the trace formula (21) contains the sum over the quantal levels where $p_n = \sqrt{E_n - \frac{1}{4}}$ is the momentum of an eigenstate; it is the quantum mechanical side of the trace formula. The function $h(p)$ is an even test function which is arbitrary except that it must be holomorphic in a strip $|\,\mathrm{Im}\; p\,| \leq \frac{1}{2} + \varepsilon$, $\varepsilon > 0$, and must decrease faster than $|p|^{-2}$ for $|p| \to \infty$. The Fourier transform of $h(p)$ is denoted by

$$g(x) \;=\; \frac{1}{2\pi} \int_{-\infty}^{\infty} dp\; e^{i\,p\,x}\; h(p) \quad . \qquad (22)$$

The right–hand side of (21) is the classical side of the trace formula containing only classical quantities like the lengths $l(t)$ and the characters $\chi(t)$ corresponding to the elements $t \in \Gamma$. The sum over the conjugacy classes of the reflection group Γ is splitted according to the special properties of its elements t. The first term on the right–hand side is the so–called zero–length contribution arising from the identity element of Γ. This contribution is also present in Gutzwiller's semiclassical trace formula [2]. The following term is due to the reflection elements t_{inv} of Γ. The next term deals with the elliptic elements $t_{\mathrm{ellip}} \in \Gamma$ where t_{ellip} corresponds to a rotation around $\frac{2\pi}{m_t}$ at a corner point having an angle of $\frac{\pi}{m_t}$. The sum over t_{sing} goes over the singular periodic orbits which are running along the edges of the billiard and deserve a special treatment. Elements t belonging to an even or odd number of reflections are denoted as t_{even} and t_{odd}, respectively. The last sum over t_{hyp} is the usual periodic orbit contribution also occurring in the generalized trace formula [26], where $\sigma(t) = 1$ for t direct hyperbolic, and $\sigma(t) = -1$ for inverse hyperbolic elements $t \in \Gamma$.

The trace formula (21) is an exact relation between quantum and classical mechanics in the case of billiard $\mathcal{B}$, whereas an exact derivation is not possible for billiard $\mathcal{A}$ for which the boundary conditions are not compatible with the reflection group Γ. In this case one is left to use Gutzwiller's semiclassical trace formula. A comparison shows that only the two sums over t_{inv} and t_{ellip} are missing in the standard form of the Gutzwiller trace formula. In the following we shall assume that possible missing terms in the trace formula (21) in case of billiard $\mathcal{A}$ do not alter our main conclusions. To make this plausible, consider for $h(p)$ the following admissible function [27]

$$h(p) \;=\; \frac{1}{2} \left\{ \mathrm{erf}\left(\frac{p'-p}{\varepsilon} \right) \;+\; \mathrm{erf}\left(\frac{p'+p}{\varepsilon} \right) \right\} \quad , \quad \varepsilon > 0 \quad , \qquad (23)$$

which yields together with (21) the spectral staircase $\mathcal{N}(E)$ in the limit $\varepsilon \to 0$. It is instructive to derive Weyl's law (5) with (23). The area term proportional to E is provided by the zero–length term. Furthermore this term produces a constant contribution of $-\frac{1}{288}$ to Weyl's law.

The perimeter term proportional to $\sqrt{E}$ is generated exactly by the sum over the reflections $t_{\rm inv}$. An additional constant contribution is eventually produced by the sum over the elliptic elements $t_{\rm ellip}$. The sums over the periodic orbits, i. e., over $t_{\rm sing}$ and $t_{\rm hyp}$, yield the oscillatory fluctuations around Weyl's law which describes only the mean behaviour. The first two terms of Weyl's law obtained in this way are identical to the first two terms in (5) for billiard $\mathcal{A}$ as well as for billiard $\mathcal{B}$. For the constant σ one obtains $\sigma = -\frac{73}{576} = -0.1267\ldots$ in the case of billiard $\mathcal{B}$, being in excellent agreement with our fit value of -0.125 (see section III.1). Applying trace formula (21) to billiard $\mathcal{A}$, where it cannot be derived exactly, gives for the constant term $\sigma = -\frac{65}{576} = -0.1128\ldots$ which does not agree so well with our fit value -0.188; nevertheless the order of magnitude is well matched. This may provide a hint that the unknown corrections are very small in this case.

IV.2 The Trace of the Cosine–Modulated Heat Kernel

The trace of the cosine–modulated heat kernel was introduced in [28, 29] to investigate the questions related to "inverse quantum chaology", i. e., the study of the periodic orbits in terms of the quantal levels. (For applications, see [30].) It is obtained from the test function

$$h(p) \;=\; \cos(pL)\, e^{-\beta E} \quad , \quad E = p^2 + \frac{1}{4} \quad , \tag{24}$$

whose Fourier transform reads

$$g(x) \;=\; \frac{e^{-\beta/4}}{4\sqrt{\pi\beta}} \left\{ e^{-(L-x)^2/4\beta} \;+\; e^{-(L+x)^2/4\beta} \right\} \quad , \tag{25}$$

where $\beta > 0$ and $L \in \mathbf{R}$. The Fourier transform (25) has the nice property that it generates on the right–hand side of the trace formula (21) Gaussian peaks of width $\Delta L \sim 2\sqrt{2\beta}$ exactly at the lengths $l(t)$ of the classical periodic orbits. The peaks are positive or negative depending on the character $\chi(t)$ of the periodic orbit. Thus one can obtain the length spectrum by evaluating the left–hand side using the computed quantal levels.

Let us consider for fixed $\beta > 0$ the following function of L

$$\begin{aligned} \Theta^C(L) \;:=\; & \sum_{n=1}^{N} \cos(p_n L)\, e^{-\beta E_n} \\ & - \int_0^{p_N} dp\; \cos(pL) e^{-\beta E} \left\{ \frac{p \tanh \pi p}{48} + \frac{1}{4\pi} \sum_{t_{\rm inv}} \chi(t) l(t) \right. \\ & \left. + \sum_{t_{\rm ellip}} \sum_{k=1}^{m_t - 1} \frac{\chi^k(t)}{4 m_t \sin(\frac{\pi k}{m_t})} \frac{\cosh(\pi p(1 - 2k/m_t))}{\cosh(\pi p)} \right\} \quad , \end{aligned} \tag{26}$$

where we have subtracted from the sum over the computed quantal levels, i. e., the left–hand side of eq.(21), the zero–length term, the sum over the reflection elements $t_{\rm inv}$, and the sum over the elliptic elements $t_{\rm ellip}$. It follows from the trace formula that $\Theta^C(L)$ is given by the remaining two sums over $t_{\rm sing}$ and $t_{\rm hyp}$ on the right–hand side, and thus should show Gaussian peaks at the locations of the various periodic orbits. Ideally, one would like to consider the limit $\beta \to 0$, but since only a finite part $\{E_n\}_{n \le N}$ of the energy spectrum is known, the smallest value of β is determined by the largest computed quantal level, in our case $E_N \simeq 100\,000$, yielding $\beta = 0.00005$. Figure 10 presents $\Theta^C(L)$ for billiard $\mathcal{A}$ (full curve) and for billiard $\mathcal{B}$ (dotted

curve) up to $L = 10$ computed from the first N quantal levels. The first lengths of periodic orbits are well resolved, but with increasing length the length–spacing between neighbouring lengths decreases and the peaks soon overlap. The differences between the two curves are due to the different characters $\chi(t)$ for billiards $\mathcal{A}$ and $\mathcal{B}$ determined by the different boundary conditions. The only possibility for further differences is the fact that the trace formula is not exact in the case of billiard $\mathcal{A}$.

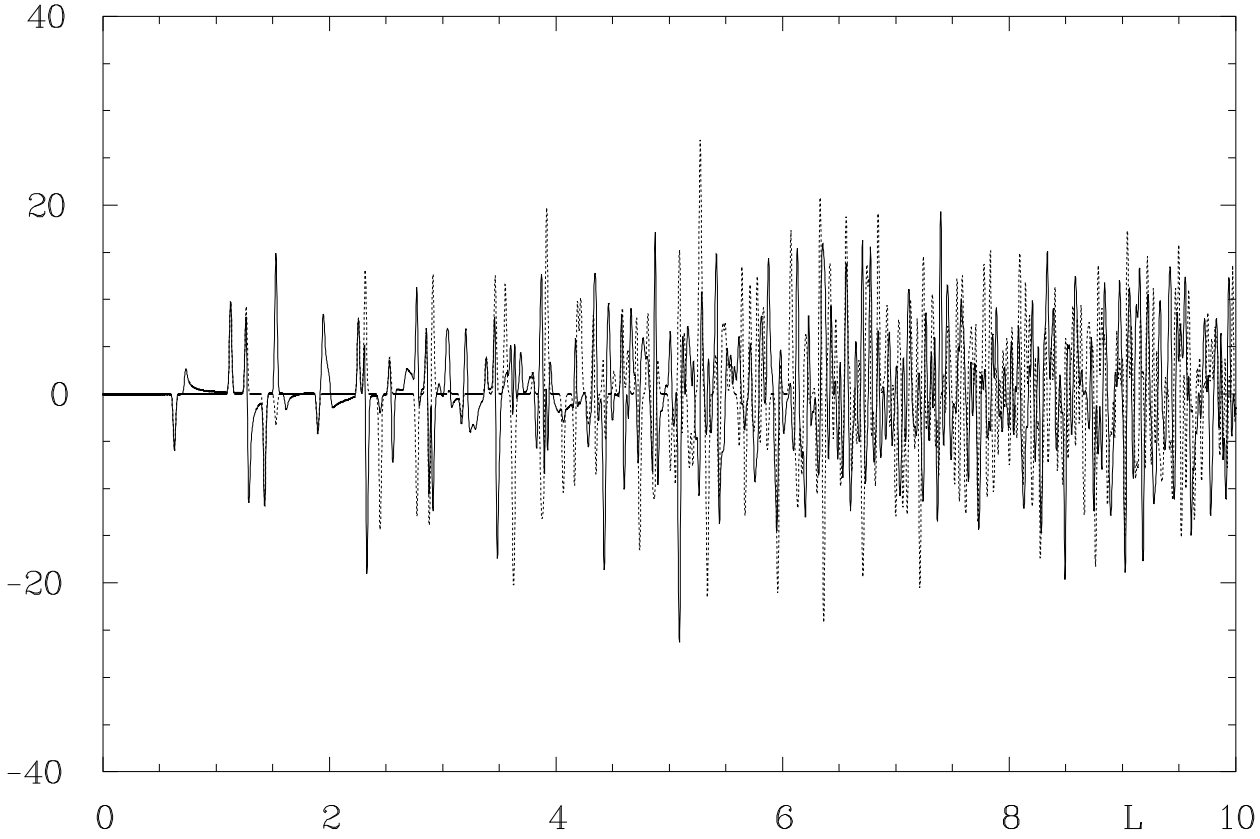

Figure 10: The trace of the cosine–modulated heat kernel $\Theta^C(L)$ is presented for billiard $\mathcal{A}$ (full curve) and billiard $\mathcal{B}$ (dotted curve) with $\beta = 0.00005$ computed from the quantal levels.

The peculiar properties of arithmetical chaos are ascribed to the exponential increase of the mean multiplicities of their length spectra [9, 12, 14, 15]. But the mean multiplicities with respect to the lengths are identical for billiard $\mathcal{A}$ and $\mathcal{B}$, and there arises the delicate question about the origin of the different level statistics for billiards $\mathcal{A}$ and $\mathcal{B}$ as discovered in section III. There is the possibility that in the case of billiard $\mathcal{A}$ the "effective" multiplicity $g_n^{\text{eff}} := g_n^+ - g_n^-$ is not exponentially increasing in the sense that for a given length the number of orbits with positive character nearly equals the number of orbits of negative character such that the effective multiplicity g_n^{eff} does not show any exponential behaviour. Since it is the effective multiplicity which enters in the spectral form factor, the different spectral behaviours would be explained by this difference. In the case of such a cancellation effect for billiard $\mathcal{A}$, the periodic orbit theory for this billiard would see much fewer periodic orbits, and Huber's law for the number of effective periodic orbits would be the standard one but with a topological entropy of one half. If such an effect is occurring in billiard $\mathcal{A}$, the trace of the cosine–modulated heat kernel should behave completely different in both cases. The peaks at the locations of the lengths of periodic orbits are proportional to g_n^{eff}. Thus one would expect for billiard $\mathcal{A}$ much smaller

peaks than for billiard $\mathcal{B}$ where an exponential $g_n^{\rm eff}$ is needed. To test this possibility, we show in figure 11 the smoothed average of the modulus of $\Theta^C(L)$, i.e., $\left\langle \left| \Theta^C(L) \right| \right\rangle$, where the full curve belongs to billiard $\mathcal{A}$ and the dashed one to billiard $\mathcal{B}$. Surprisingly, both curves behave very similar and fluctuate for $L > 5$ around a plateau. Thus our data do not seem to support the idea that a cancellation effect between periodic orbits of the same length occurs in billiard $\mathcal{A}$. One therefore concludes that solely from the exponential increase of the multiplicities one cannot derive Poissonian level fluctuations. Since the periodic–orbit theory should describe the level fluctuations correctly, it seems that the simple models [12, 15] considered so far are too much simplified. It appears that a refined model would require more detailed information on the characters; the different level statistics for billiard $\mathcal{A}$ and $\mathcal{B}$ must be determined by the subtle differences with respect to their characters.

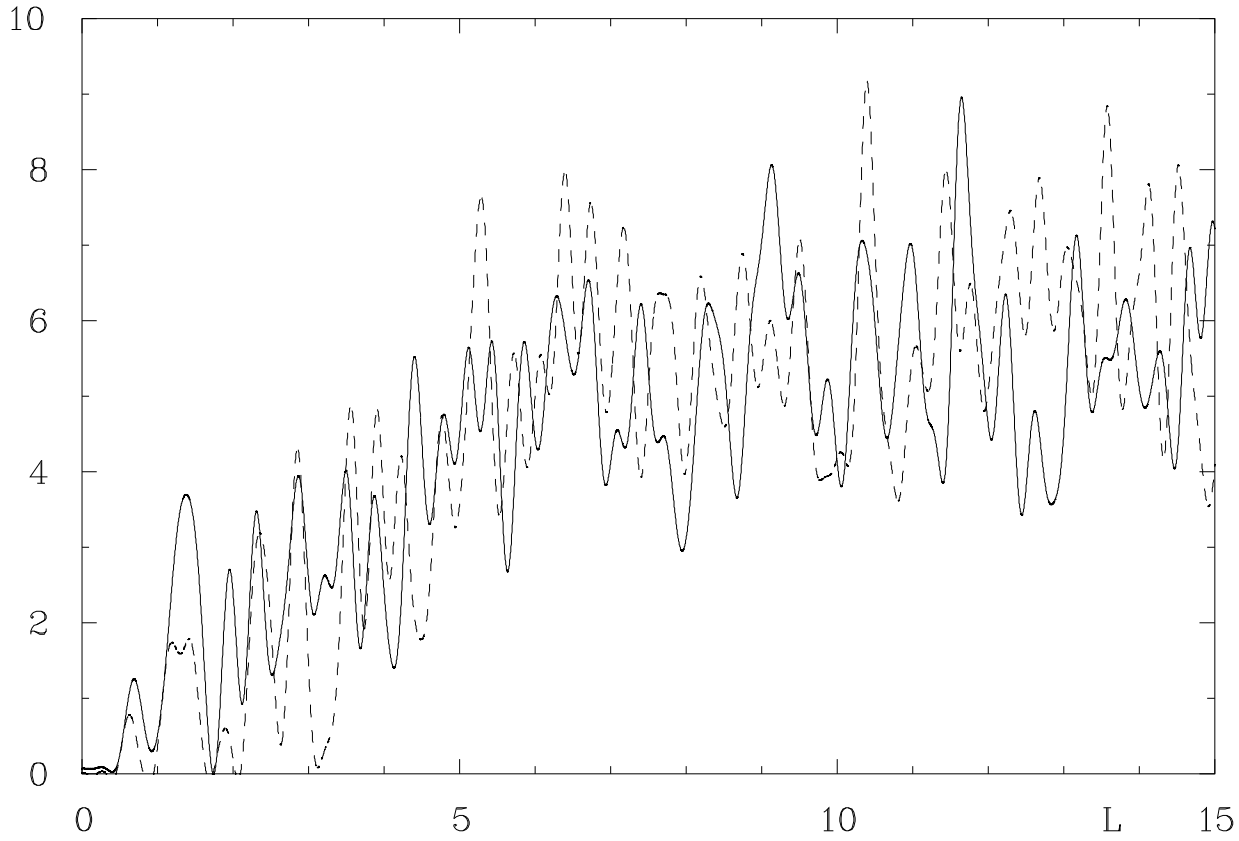

Figure 11: $\left\langle \left| \Theta^C(L) \right| \right\rangle$ is shown for billiard $\mathcal{A}$ (full curve) and for billiard $\mathcal{B}$ (dashed curve).

IV.3 The Semiclassical Spectral Form Factor

The spectral form factor $K(\tau)$ was introduced in the framework of random–matrix theory for a convenient description of level fluctuations. Defined as $K(\tau) := 1 - b(\tau)$, where $b(\tau)$ is the Fourier transform of the two–level cluster function $Y_2(r)$ [31], it is related to the number variance by the integral transform [20]

$$\Sigma^2(L) \;=\; \frac{2}{\pi^2} \int_0^\infty d\tau \, \frac{\sin^2(\pi L \tau)}{\tau^2} \, K(\tau) \quad . \tag{27}$$

The spectral form factor allows a study of the level fluctuations in terms of the periodic orbits. A semiclassical approximation leads to [5]

$$K_{\rm sc}(\tau) \;=\; \frac{1}{\overline{d}(\overline{E})} \int_{-\infty}^{\infty} d\varepsilon \;\langle\, d_{\rm fl}(E-\varepsilon/2)\, d_{\rm fl}(E+\varepsilon/2)\,\rangle_{\overline{p},\Delta p}\; e^{2\pi i \overline{d}(\overline{E})\varepsilon\tau} \quad , \tag{28}$$

where $\overline{d}(E)$ and $d_{\rm fl}(E)$ are the mean and the fluctuating part of the spectral density $d(E)$, respectively. Expressing $d_{\rm fl}(E)$ by its periodic–orbit expression derived from the trace formula and inserting this in eq.(28) allows the application of periodic–orbit theory to the study of quantal level statistics. Evaluating the integral in (28) by the method of stationary phase leads to

$$K_{\rm sc}(\tau) \;=\; \frac{1}{4\pi\,\overline{d}(\overline{E})} \left\langle \sum_t \sum_{k=-\infty}^{\infty}{}' \sum_{t'} \sum_{k'=-\infty}^{\infty}{}' \frac{A(t,k)\; A^{\star}(t',k')}{p} \right.$$
$$\left. e^{ip(kl(t)-k'l(t'))}\; \delta\left(\ell - \frac{1}{2}(kl(t)+k'l(t'))\right) \right\rangle_{\overline{p},\Delta p} \quad , \tag{29}$$

where the amplitudes $A(t,k)$ of the periodic orbits can be read off from the trace formula (21), and

$$\ell \;:=\; 4\pi p \overline{d}(E)\;\tau \quad . \tag{30}$$

The prime at the k–sum counting positive and negative traversals denotes that $k=0$ is excluded. Assuming for the average $\langle \ldots \rangle$ a Gaussian average around the momentum $\overline{p}$ with width Δp,

$$\langle\; f(p)\;\rangle_{\overline{p},\Delta p} \;:=\; \int_{-\infty}^{\infty} dp\; \frac{1}{\sqrt{2\pi}\Delta p}\; e^{-\frac{(p-\overline{p})^2}{2\Delta p^2}}\; f(p) \quad , \tag{31}$$

one obtains

$$K_{\rm sc}(\tau) \;=\; \frac{1}{4\pi\overline{d}(\overline{E})} \sum_t \sum_{k=-\infty}^{\infty}{}' \sum_{t'} \sum_{k'=-\infty}^{\infty}{}' \frac{A(t,k)\; A^{\star}(t',k')}{\overline{p}}$$
$$\frac{1}{\sqrt{2\pi}\Delta p \mu}\; e^{i(kl(t)-k'l(t'))\frac{\overline{l}}{\mu}}\; e^{-\frac{(\overline{l}/\mu-\overline{p})^2}{2\Delta p^2}} \quad , \tag{32}$$

with $\mu := 4\pi\overline{d}(\overline{E})\tau$ and $\overline{l} := \frac{1}{2}(kl(t)+k'l(t')\,)$.

Now we would like to discuss the so–called diagonal approximation of (32) which plays a central role in all explanations of the peculiar behaviour of arithmetical chaos. The diagonal approximation $K_{\rm sc}^{\rm D}(\tau)$ consists of replacing the quadruple sum in (32) by the double sum over the diagonal elements $t=t'$ and $k=k'$, which should be justified for very small values of τ, such that $K_{\rm sc}(\tau) \simeq K_{\rm sc}^{\rm D}(\tau)$ in the range of validity. In the case of a chaotic system possessing only time reversal symmetry without arithmetical properties, one has $K_{\rm sc}^{\rm D}(\tau) = 2\tau$ which agrees with the small–τ behaviour of the GOE form factor, $K_{\rm GOE}(\tau) \;\sim\; 2\tau$, see eq.(43) below. For systems with arithmetical chaos one expects in contrast an exponentially increasing spectral form factor at least for those small values of τ where the diagonal approximation is justified. This is the basis for the explanation of the special properties of arithmetical chaos [12, 15]. To derive the diagonal approximation in the arithmetical case, we replace $A(t,k)$ by its asymptotic value $A(t,k) \simeq \chi(t)^k l(t) e^{-kl(t)/2}$ and sum over distinct lengths, i. e., we take into account the mean degeneracy $\langle g(l)\rangle = c_\Gamma e^{l/2}/l$ and use $N_{\rm distinct}(l) = \frac{2}{c_\Gamma} e^{l/2}$, which leads to

$$K_{\rm sc}^{\rm D}(\tau) \;=\; \frac{c_\Gamma}{4\pi\overline{d}(\overline{E})} \int_{l_0}^{\infty} dl\; e^{l/2}\; \frac{1}{\sqrt{2\pi}\Delta p}\; e^{-\frac{(l/\mu-\overline{p})^2}{2\Delta p^2}} \quad , \tag{33}$$

where l_0 denotes the shortest length. This is the diagonal approximation for a finite energy averaging. To obtain the result in [12, 15], the limit $\Delta p \to 0$ has to be considered, in which the Gaussian in the integral including its prefactor gives a δ–distribution. This leads to

$$K_{\rm sc}^{\rm D}(\tau) \;=\; \frac{c_\Gamma}{4\pi \overline{d}(\overline{E})\overline{p}}\; e^{2\pi \overline{d}(\overline{E})\overline{p}\tau} \quad . \tag{34}$$

In [12, 15] it is assumed that the true spectral form factor shows for small τ exactly this exponential behaviour until it reaches the saturation value 1, and thus one arrives at the following simplified model for the spectral form factor

$$K_{\rm model}(\tau) \;:=\; \min\left(\,1\,,\,\frac{c_\Gamma}{4\pi \overline{d}(\overline{E})\overline{p}}\; e^{2\pi \overline{d}(\overline{E})\overline{p}\tau}\right) \quad . \tag{35}$$

One sees that (35) reaches the value one at

$$\tau_d \;=\; \frac{1}{2\pi \overline{d}(\overline{E})\overline{p}}\;\log\left(\frac{4\pi \overline{d}(\overline{E})\overline{p}}{c_\Gamma}\right) \quad , \tag{36}$$

which is the maximal τ–value up to which the diagonal approximation must be employed. With (27) one can predict the number variance using the model form factor (35) and the spectral rigidity using (14).

Let us now turn to the crucial question whether the diagonal approximation is justified at all in the case of finite–energy averaging $\Delta p > 0$. Eq.(32) shows that each term contributes a Gaussian $\exp(-(\overline{l}/\mu - \overline{p})^2/(2\Delta p^2)\,)$. Thus the diagonal approximation breaks down if the width of the Gaussian is comparable to the distance between neighbouring Gaussians. Since we need the width of the Gaussian in τ, we Taylor expand the argument of the Gaussian having the form

$$\exp\left(-\frac{1}{2\sigma^2}\;\left(\frac{1}{\tau}-\frac{1}{\tau_0}\right)^2\right) \;\simeq\; \exp\left(-\frac{1}{2\sigma^2\tau_0^4}\;(\tau-\tau_0\,)^2\right) \;=:\; \exp\left(-\frac{1}{2\Delta\tau^{\,2}}\,(\tau-\tau_0\,)^2\right) \tag{37}$$

being valid up to order $O(\,(\tau-\tau_0)^3\,)$. One concludes that the Gaussian has a width of approximately

$$\Delta\tau \;=\; \frac{\overline{l}\Delta p}{4\pi\overline{p}^2\overline{d}(\overline{E})} \quad , \tag{38}$$

which by means of (30) corresponds to a "length width" of $\Delta l = \frac{\Delta p}{\overline{p}} l$. Since the distance between neighbouring lengths is approximately given by $\Delta l = c_\Gamma e^{-l/2}$, one obtains overlapping Gaussians at a length given by the transcendental equation

$$\widehat{l}\, e^{\widehat{l}/2} \;=\; c_\Gamma \frac{\overline{p}}{\Delta p} \quad . \tag{39}$$

This determines the maximal length and with (30) the maximal τ–value $\widehat{\tau}$ at which the diagonal approximation is an appropriate description of the spectral form factor. To justify the model form factor (35), it is necessary that the diagonal approximation is valid up to τ_d, defined in (36). Thus for a given energy averaging at $\overline{p}$ with width Δp one must require $\tau_d < \widehat{\tau}$. From the condition (39) follows that in the limit $\Delta p \to 0$ the diagonal approximation is valid for an increasing τ–interval, such that (35) is justified in this limit. However, the breakdown can be caused by a finite value of Δp as it is required for any application.

For a numerical evaluation of the spectral form factor $K(\tau)$ in terms of the quantal levels it is convenient to employ a semiclassical approximation which is obtained from (29) by a Gaussian averaging in p followed by an additional Gaussian averaging in τ yielding the relation [32, 33]

$$K_{\rm sc}(\tau) \;=\; \frac{\Delta p}{(2\pi)^{3/2}\overline{p}\,\overline{d}(\overline{E})} \left| \sum_t \sum_{k=-\infty}^{\infty}{}' A(t,k)\, \exp\left(i\overline{p}kl(t)\right)\, \exp\left(-\Delta p^2\left(\ell - kl(t)^2\right)\right) \right|^2 \quad . \quad (40)$$

Although formula (40) was originally derived to extract information from the periodic orbits, one can also reverse the point of view with the help of the trace formula (21). This is possible because the quadruple sum which naturally occurs in the periodic–orbit expression for $K_{\rm sc}(\tau)$ is in eq.(40) effectively reduced to a double periodic–orbit sum. (Note, however, that a quadruple sum is still present because of the modulus square.) An exact periodic–orbit expression for $K(\tau)$ has been derived in [34]. But since it is not possible to reduce the quadruple sum in this exact expression, one cannot evaluate the exact formula using the quantal levels via the trace formula (21). Thus we shall now use the semiclassical expression (40). To express the periodic–orbit sum in terms of the quantal levels we choose in the trace formula

$$h(p) \;=\; \frac{\sqrt{\pi}}{\Delta p}\left\{ \exp\left(-\frac{(p-\overline{p})^2}{4\Delta p^2} - i(p-\overline{p})\ell\right) \;+\; \exp\left(-\frac{(p+\overline{p})^2}{4\Delta p^2} - i(p+\overline{p})\ell\right)\right\} \quad (41)$$

whose Fourier transform reads

$$g(x) \;=\; \exp(-\Delta p^2(\ell-x)^2 + i\overline{p}x) \;+\; \exp(-\Delta p^2(\ell+x)^2 - i\overline{p}x) \quad . \quad (42)$$

The Fourier transform (42) is exactly the expression which occurs in (40). Thus we can identify the periodic–orbit sum in eq.(40) with the corresponding sum in the trace formula (21) which in turn allows us to replace the sum over periodic orbits by the left–hand side of the trace formula, i.e., by a sum over the quantal energies. In our numerical evaluation we subtract from the sum over the quantal levels the zero–length contribution, the sum over the reflection elements $t_{\rm inv}$ and the sum over the elliptic elements $t_{\rm ellip}$. Then only the periodic orbit sum is obtained. To justify this subtraction, note, that $d_{\rm fl}(E)$ occurs in eq.(28). Since the zero–length term corresponds to the area term and part of the constant in Weyl's law, the sum over the reflection elements to the perimeter term, and the sum over the elliptic elements to the other part of the constant, one has indeed computed the contributions to $d_{\rm fl}(E)$.

The obtained spectral form factor is connected with the number variance defined by a Gaussian averaging at momentum $\overline{p}$ and width Δp (instead of the rectangular averaging used in section III.3). In the following two different energy ranges are studied: a low–energy range defined by $\overline{p} = 150$, $\Delta p = 15$, and a high–energy range defined by $\overline{p} = 270$, $\Delta p = 10$. The spectral form factor is a rapidly fluctuating function. As an example figure 12 presents the spectral form factor for billiard $\mathcal{B}$ at $\overline{p} = 270$. The strong fluctuations are not an artifice of the employed approximations since this behaviour has also been observed for the exact spectral form factor [34]. Because the strong fluctuations hide the mean properties, we average the spectral form factor such that the wildest fluctuations are suppressed. The result is shown in figure 13 for the two billiards in the low– as well as in the high–energy range. In all four cases the spectral form factor saturates for $\tau > 1$ and fluctuates around the value one which exemplifies the fact that formula (40) deals in fact with a quadruple sum, i.e., it includes non–diagonal contributions, since it would otherwise display the behaviour of the diagonal approximation which always increases with τ. The GOE spectral form factor

$$K_{\rm GOE}(\tau) \;=\; \begin{cases} 2\tau - \tau\ln(1+2\tau) & , \quad 0 \le \tau \le 1 \\ 2 - \tau\ln\left(\frac{2\tau+1}{2\tau-1}\right) & , \quad \tau \ge 1 \end{cases} \quad (43)$$

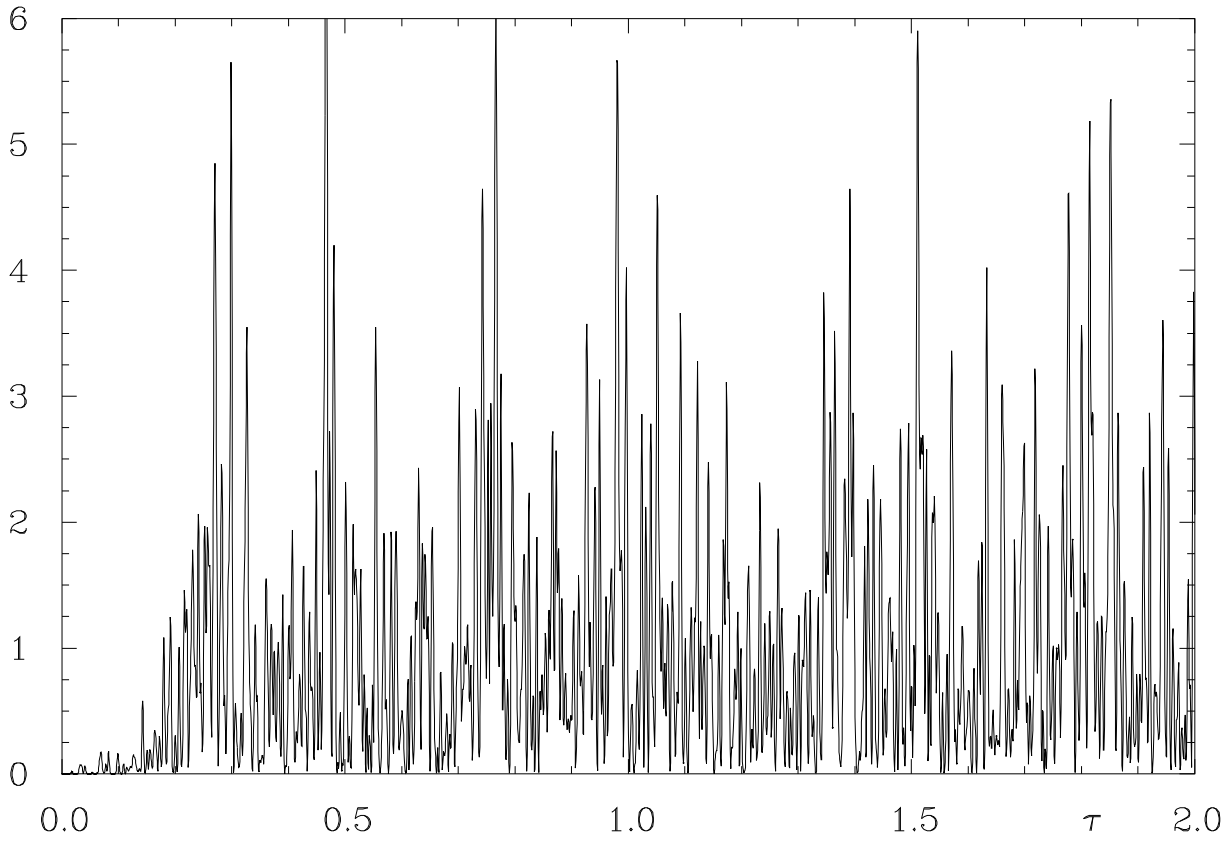

Figure 12: The spectral form factor is shown for billiard $\mathcal{B}$ with the parameters $\overline{p} = 270$ and $\Delta p = 10$.

is also shown in figures 13a and 13b dealing with billiard $\mathcal{A}$. Despite the fluctuations, rough agreement is observed. This also demonstrates the stationarity of the level fluctuations for billiard $\mathcal{A}$.

A completely different behaviour is revealed for $\tau < 1$ for billiard $\mathcal{B}$ where the spectral form factor increases in general much faster than the GOE behaviour. In figures 13c and 13d the model form factor (35) is shown where the value $c_\Gamma = \frac{1}{1+\sqrt{2}}$ is used. A surprisingly good agreement with the mean behaviour of the spectral form factor is observed. Note, however, that the same model spectral form factor should also describe billiard $\mathcal{A}$. There remains the question why this argumentation leads to a satisfactory description for billiard $\mathcal{B}$ and not for billiard $\mathcal{A}$ having the same multiplicities. Using eq.(39) one obtains for $\overline{p} = 150$ and $\Delta p = 15$ the value $\widehat{\tau} = 0.0885$ up to which the diagonal approximation is justified, whereas in the case of the model form factor the diagonal approximation is employed up to $\tau_d = 0.393$. This shows that the diagonal approximation is not valid over practically the whole τ–interval. The inapplicability of the model form factor is even more obvious if one notes that $K_{\rm sc}^{\rm D}(\widehat{\tau}) \simeq 0.050$, whereas the GOE form factor is at the same $\widehat{\tau}$–value already as large as $K_{\rm GOE}(\widehat{\tau}) \simeq 0.177$. Here arises the odd situation that the diagonal approximation of the form factor, which should explain by its fast increasing behaviour the peculiar spectral statistics, is actually smaller than the GOE form factor. One faces a similar situation in the higher energy range, i. e., for $\overline{p} = 270$ and $\Delta p = 10$, where one gets $\widehat{\tau} = 0.0787$ and $\tau_d = 0.256$ together with $K_{\rm sc}^{\rm D}(\widehat{\tau}) \simeq 0.047$ and $K_{\rm GOE}(\widehat{\tau}) \simeq 0.157$. One thus concludes that the diagonal approximation is not valid in both cases. Nevertheless, it is very strange to observe in figures 13c and 13d a much better agreement

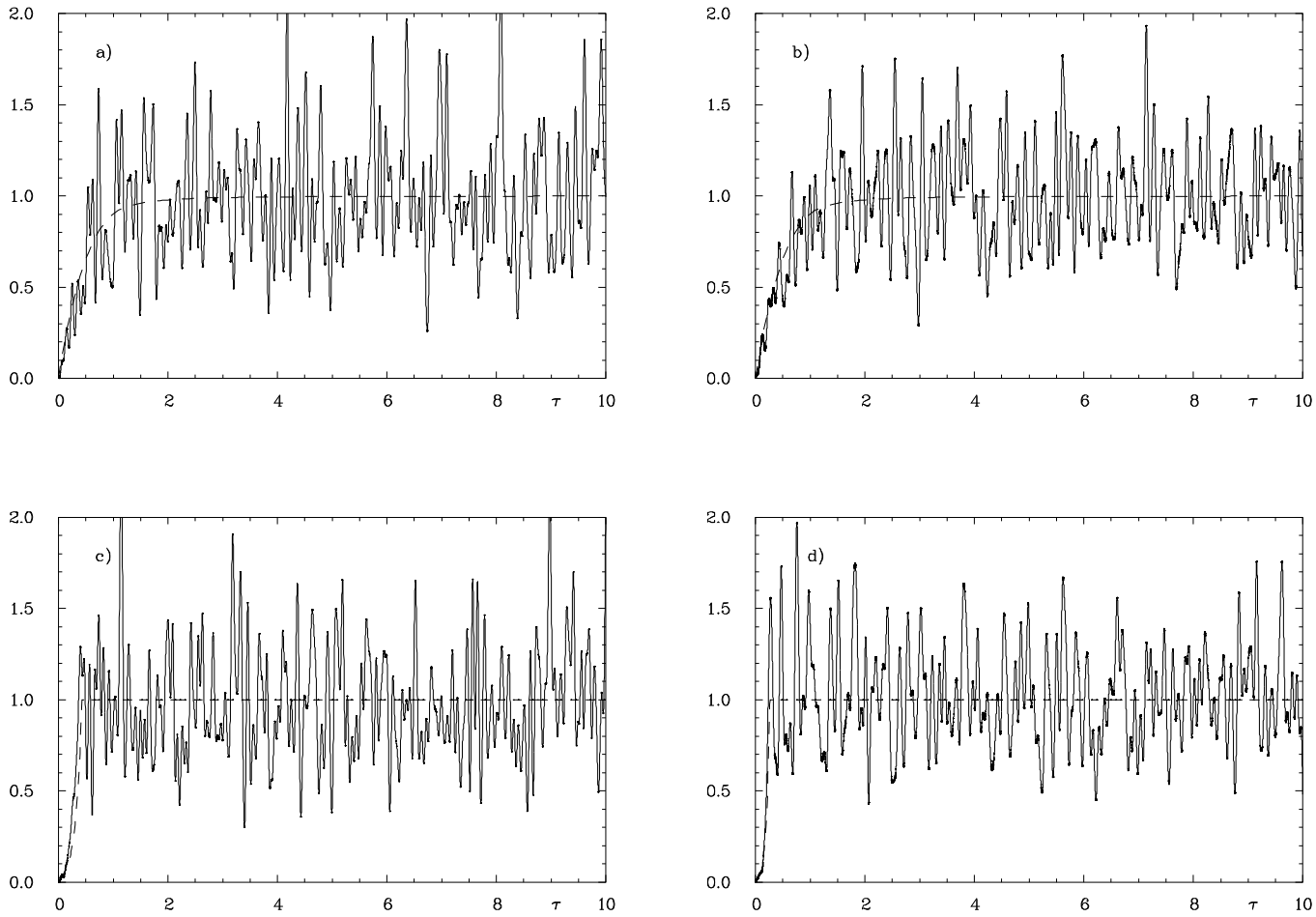

Figure 13: The smoothed spectral form factor is shown for billiard $\mathcal{A}$ in figures a) ($\overline{p} = 150, \Delta p = 15$) and b) ($\overline{p} = 270, \Delta p = 10$) in comparison with the GOE spectral form factor (43) (dashed curve). Figures c) ($\overline{p} = 150, \Delta p = 15$) and d) ($\overline{p} = 270, \Delta p = 10$) display the smoothed spectral form factor for billiard $\mathcal{B}$ in comparison with the exponential model form factor (35) (dashed curve) discussed in the text.

with the model form factor than with the GOE form factor, which contrasts to figures 13a and 13b which show a good agreement with the GOE form factor. Since the model form factor is neither applicable nor able to explain the differences in the energy spectra of the two billiards, there must be another origin of the differences. One possibility could be a strange correlation between the characters of neighbouring orbits in such a way that the different spectral form factors are generated, where, however, the contributions of non–diagonal elements must play a significant role. Finally, we would like to point out that the cosine–modulated heat kernel was not able to clearly distinguish the two billiards, whereas the spectral form factor indeed shows a different behaviour for $\tau < 1$. The form factor is thus the most suited quantity on which a correct theory of arithmetical quantum chaos should be built.

Since the spectral form factor (40) is based on a semiclassical approximation, it is important to check also the validity of (40) at least numerically. To this aim we computed the number variance $\Sigma^2(L)$ using the spectral form factor (40) in the integral equation (27). The results are compared with the "true" number variance which is obtained by averaging the number variance of the quantal levels at 5000 random sample points p which in turn are Gaussian distributed

according to $\overline{p}$ and Δp. The results shown in figure 14 demonstrate that the approximation is at least numerically justified.

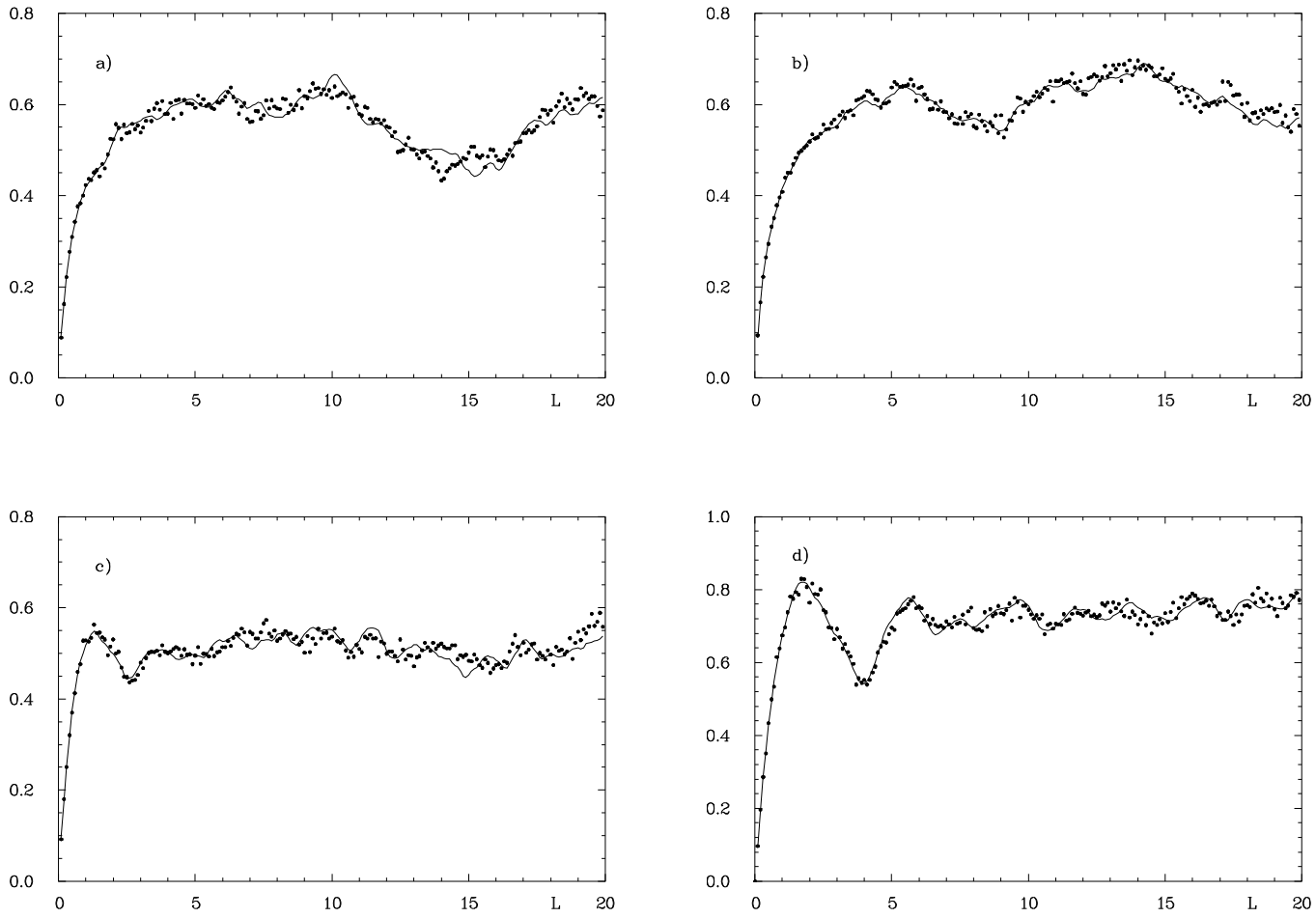

Figure 14: The number variance $\Sigma^2(L)$ is shown for billiard $\mathcal{A}$ in a) $(\overline{p} = 150, \Delta p = 15)$ and b) $(\overline{p} = 270, \Delta p = 10)$. The full curve is obtained from the approximate spectral form factor (40) using the integral representation (27), whereas the dots are obtained directly from the quantal spectrum using 5000 sample points. Figures c) $(\overline{p} = 150, \Delta p = 15)$ and d) $(\overline{p} = 270, \Delta p = 10)$ display the same quantities for billiard $\mathcal{B}$.

V Summary and Discussion

We have studied the level statistics of two strongly chaotic quantum billiards. Since the billiard ball table was for both billiards the same non–euclidean triangle, the two billiards are classically identical in that they possess the same classical periodic orbits. They only differ in the boundary conditions imposed on the quantum mechanical wave functions which is reflected in different characters, i. e., in different signs of the amplitudes attached to the periodic orbits in the trace formula. For the triangular billiard domain we have chosen the fundamental domain of the reflection group $\mathrm{T}^\star(2,3,8)$. Since this group is an arithmetical group, the periodic orbits possess an exponentially degenerate length spectrum. The boundary conditions have been chosen in such a way that billiard $\mathcal{A}$ does not belong to a representation of the reflection group, whereas

the boundary conditions imposed on billiard $\mathcal{B}$ are compatible with an irreducible symmetry representation.

A previous analysis [17] based on the first 200 energy levels revealed for billiard $\mathcal{B}$ the peculiar level statistics characteristic for arithmetical quantum chaos. It turned out, however, that the level statistics of billiard $\mathcal{A}$ are at short– and medium–range correlations in accordance with the GOE–behaviour of random–matrix theory typically found for generic systems. There remained the important question, whether this mysterious difference between these almost identical billiards is only a low–energy effect, or whether it could be confirmed over a much larger energy range and with much better statistics.

In this paper we have extended the previous analysis using now for both billiards the first 1050 levels which we have computed using the boundary element method. Our new analysis covers the full energy range up to $E = 100\,000$. In Sec. III we have presented a detailed analysis of the level statistics which shows clearly that billiard $\mathcal{A}$ indeed behaves like a generic chaotic quantum system, while billiard $\mathcal{B}$ shows the typical behaviour of arithmetical quantum chaos.

Since the level statistics of quantum billiard $\mathcal{A}$ show all properties of generic quantum chaos, although the classical counterpart possesses the strange arithmetical structure typical for arithmetical chaos, we call this dynamical system *pseudoarithmetical* in order to distinguish it from systems like quantum billiard $\mathcal{B}$ which is a genuine *arithmetical* system showing the exceptional level statistics characteristic for arithmetical quantum chaos.

The number variance $\Sigma^2(L)$, and the spectral rigidity $\Delta_3(L)$ show for both billiards a saturation plateau at long–range correlations and thus a breakdown of the universal behaviour derived for random matrices. Of special interest is the energy–dependence of the plateau height $\Delta_\infty(E)$ which we have computed in Sec. III.4. As expected, we find that the energy dependence of $\Delta_\infty(E)$ is for the pseudoarithmetical billiard $\mathcal{A}$ in good agreement with a logarithmic increase, see figure 8, in accordance with Berry's semiclassical analysis [5] for generic chaotic systems being invariant under time reversal. It turns out, however, that a fit of the form $\Delta_\infty(E) = \frac{1}{2\pi^2}\log E + \gamma$, shown as the full curve in figure 8, gives for the constant γ a value that does not agree with the constant $c(l_0)$ in Berry's formula (15) which is solely determined by the length l_0 of the shortest periodic orbit. This agrees with an earlier analysis [34] which already showed that the precise saturation value is determined by the lower part of the length spectrum of periodic orbits, but not just by the very shortest orbit. In the case of the arithmetical billiard $\mathcal{B}$ we find that the energy dependence agrees well with the simple ansatz $\Delta_\infty(E) = \alpha\sqrt{E}+\beta$, see the dotted curve in figure 8, which generically holds for integrable systems. In [12] a $\sqrt{E}/\log E$–behaviour was derived from a simple model of arithmetical quantum chaos, a behaviour which is, however, excluded by our data. This gives a first hint that there are subtle properties of arithmetical systems which require a modification of the simple model proposed in [12].

Knowing the correct energy dependence of $\Delta_\infty(E)$ gave us the opportunity to calculate the value distribution $P(W)$ of the mode fluctuation $W(E)$ defined in eq.(17). According to a recent conjecture [21, 22], $P(W)$ should display for both billiards in the semiclassical limit the parameter–free universal Gaussian behaviour (20). The comparison presented in figures 9a and 9b gives strong support to this conjecture. The important point is that the distribution $P(W)$ gives us a universal measure for quantum chaos which depends only on whether the corresponding classical system is strongly chaotic or not, independent on whether the system is arithmetical, pseudoarithmetical or generic.

In Sec. IV we have employed the periodic–orbit theory to shed some light on the observed level statistics for billiard $\mathcal{A}$ and $\mathcal{B}$. In the case of the arithmetical quantum billiard $\mathcal{B}$, one has the exact Selberg trace formula (21) recently derived in [25], whereas for the pseudoarithmetical

quantum billiard $\mathcal{A}$, one has to rely on Gutzwiller's semiclassical trace formula [2] appropriately generalized to the non–euclidean geometry of billiard $\mathcal{A}$. In our analysis carried out in Sec. IV we have assumed that the trace formula for the pseudoarithmetical system is again given by eq.(21), but that in this case it is only semiclassically valid, i. e., we have assumed that the unknown correction terms, which have to be added to the right–hand side of eq.(21), are subdominant in the semiclassical limit and thus do not alter the main results of our analysis.

Using the computed quantal levels up to $E = 100\,000$, we have computed in Sec. IV.2 the truncated trace of the cosine–modulated heat kernel $\Theta^C(L)$, see eq.(26), for fixed $\beta = 0.00005$ as a function of L. The idea, of course, was that this function would exhibit a different behaviour depending on the arithmetical and pseudoarithmetical case, respectively. Since $\Theta^C(L)$ has an alternative representation, derived from the right–hand side of the trace formula, as a sum over periodic orbits, it could be expected that the different behaviour seen in the level statistics would find its correspondence in a different behaviour of the function $\Theta^C(L)$ for the two billiards. The results presented in figures 10 and 11 show, however, that billiard $\mathcal{A}$ and $\mathcal{B}$ behave in a very similar way. From this we have concluded that there is no cancellation effect between periodic orbits of the same length in billiard $\mathcal{A}$ that would lead to a much smaller effective multiplicity of periodic orbits in the pseudoarithmetical case compared with the exponential degeneracy in the arithmetical billiard, which in turn is thought to be responsible for the peculiar level statistics characteristic for arithmetical quantum chaos. It thus appears that the different level statistics for billiard $\mathcal{A}$ and $\mathcal{B}$ must be caused by subtle differences with respect to their characters.

To settle the question concerning the characters, we investigated in Sec. IV.3 the semiclassical spectral form factor $K_{\rm sc}(\tau)$ defined in eq.(28). (For a critical discussion of this approximation, we refer to [34].) Since the expression (28) does not allow a meaningful computation using the known energy levels, we have employed a further approximation leading to the expression (40) which can now be completely expressed in terms of the energy levels using the test function (41) in the trace formula. Using this formula we have obtained for the form factor the results shown in figures 12 and 13. Figure 12 shows that the form factor is a very spiky function, and therefore we have shown in figures 13a to 13d a smoothed version where the wildest fluctuations have been suppressed. Figures 13a and 13b show that the mean behaviour of the smoothed form factor for the pseudoarithmetical billiard $\mathcal{A}$ is in good overall agreement with the GOE form factor and thus in conformity with the generic level statistics which we have found for this billiard. In contrast, the mean behaviour of the smoothed form factor for the arithmetical billiard $\mathcal{B}$, represented in figures 13c and 13d, is in good overall agreement with the model form factor (35) whose derivation made essential use of the exponential multiplicity of the periodic orbits. Thus the spectral form factor behaves very differently for the two billiards in accordance with the different level statistics observed for billiards $\mathcal{A}$ and $\mathcal{B}$. This proves that the spectral form factor is a sensitive measure for the delicate differences between the two almost identical billiards. In particular, it demonstrates that the main difference between arithmetical and pseudoarithmetical quantum chaos is caused by subtle properties of the characters attached to the classical periodic orbits.

It is worthwhile to mention that the observation, that the characters attached to the periodic orbits show for arithmetical systems a different behaviour than for generic ones, has already been made in a previous paper [35]. There it was shown that the signs of the coefficients of the Dirichlet series expansion of the dynamical zeta function behave completely different in the case of Artin's billiard, which is arithmetical, compared to generic systems. (The signs of the Dirichlet coefficients are directly related to the characters.)

Future progress towards a deeper understanding of the subtleties of arithmetical and pseu-

doarithmetical quantum chaos may be achieved in the following three steps. In the first step one has to justify the approximate representation (40) for the spectral form factor which yields numerically reasonable results as we have demonstrated in figure 14. In the second step one has to incorporate the properties of the length spectrum and, very importantly, the subtle behaviour of the characters attached to the classical periodic orbits. Finally, in the third step, one has to extract from formula (40) the mean behaviour of the spectral form factor. As a result one would obtain an improved model for the form factor which would include non–diagonal contributions which are very essential as we have emphasized in Sec. IV.3. From the new form factor one could then compute the various level statistics. We hope to return to these points in a later publication.

Acknowledgment

It is a pleasure to thank H. Ninnemann for helpful discussions. Furthermore, we would like to thank the Deutsche Forschungsgemeinschaft for financial support.

References

[1] M. L. Mehta, *Random Matrices and the Statistical Theory of Energy Levels* (Academic Press, New York, 1967) and new revised and enlarged edition, 1990.

[2] M. C. Gutzwiller, *Chaos in Classical and Quantum Mechanics* (Springer, New York, 1990).

[3] O. Bohigas, M.–J. Giannoni, and C. Schmit, Phys. Rev. Lett. **52**,1 (1984).

[4] O. Bohigas, M.–J. Giannoni, and C. Schmit, J. Physique Lett. **45**, L–1015 (1984).

[5] M. V. Berry, Proc. R. Soc. Lond. **A 400**, 229 (1985).

[6] O. Bohigas, M.–J. Giannoni, and C. Schmit, *Spectral Fluctuations, Random Matrix Theories and Chaotic Motion*, in Lecture Notes in Physics Vol. 262 (Springer, Heidelberg, 1986).

[7] R. Aurich and F. Steiner, Physica **D 43**, 155 (1990).

[8] N. L. Balazs and A. Voros, Phys. Rep. **143**, 109 (1986).

[9] R. Aurich and F. Steiner, Physica **D 32**, 451 (1988).

[10] R. Aurich, E. B. Bogomolny, and F. Steiner, Physica **D 48**, 91 (1991).

[11] J. Bolte, Nonlinearity **6**, 935 (1993).

[12] J. Bolte, Int. J. of Mod. Phys. **B 7**, 4451 (1993).

[13] C. Matthies and F. Steiner, Phys. Rev. **A 44**, R7877 (1991).

[14] J. Bolte, G. Steil, and F. Steiner, Phys. Rev. Lett. **69**, 2188 (1992).

[15] E. B. Bogomolny, B. Georgeot, M.–J. Giannoni, and C. Schmit, Phys. Rev. Lett. **69**, 1477 (1992).

[16] G. Steil, DESY–report DESY 94–028 (March 1994), submitted to Math. Comp.

[17] R. Aurich, Ph. D. Thesis, Universität Hamburg, 1990.

[18] A. Selberg, J. Indian Math. Soc. **20**, 47 (1956).

[19] R. Aurich and F. Steiner, Physica **D 64**, 185 (1993).

[20] F. J. Dyson and M. L. Mehta, J. Math. Phys. **4**, 701 (1963).

[21] F. Steiner, in *Schlaglichter der Forschung. Zum 75. Jahrestag der Universität Hamburg 1994*, pp. 543, edited by R. Ansorge (Reimer, Berlin and Hamburg, 1994).

[22] R. Aurich, J. Bolte, and F. Steiner, Phys. Rev. Lett. **73**, 1356 (1994).

[23] D. R. Heath–Brown, Acta Arithmetica **LX.4**, 389 (1992);
P. M. Bleher, Z. Cheng, F. J. Dyson, and J. L. Lebowitz, Commun. Math. Phys. **154**, 433 (1993);
P. M. Bleher, D. V. Kosygin, and Y. G. Sinai, Princeton preprint (July 1994).

[24] A. Selberg, Arch. Math. Naturvid. **B 48**, 89 (1946);
A. Ghosh, J. Number Theory **17**, 93 (1983);
H. L. Montgomery, in *Number Theory, Trace Formulas and Discrete Groups*, pp. 157, edited by K. E. Aubert, E. Bombieri, and D. Goldfeld (Academic, New York, 1989).

[25] H. Ninnemann, Ph. D. Thesis, Universität Hamburg, 1994.

[26] M. Sieber and F. Steiner, Phys. Lett. **A 144**, 159 (1990).

[27] R. Aurich, C. Matthies, M. Sieber, and F. Steiner, Phys. Rev. Lett. **68**, 1629 (1992).

[28] R. Aurich, M. Sieber, and F. Steiner, Phys. Rev. Lett. **61**, 483 (1988).

[29] R. Aurich and F. Steiner, Physica **D 39**, 169 (1989).

[30] R. Aurich and F. Steiner, Phys. Rev. **A 45**, 583 (1992).

[31] F. J. Dyson, J. Math. Phys. **3**, 166 (1962).

[32] N. Argaman, Y. Imry, and U. Smilansky, Phys. Rev. **B 47**, 4440 (1993).

[33] R. Aurich and M. Sieber, J. Phys. **A 27**, 1967 (1994).

[34] R. Aurich and F. Steiner, DESY–report DESY 94–058 (March 1994),
submitted to Physica **D**.

[35] R. Aurich, J. Bolte, C. Matthies, M. Sieber, and F. Steiner, Physica **D 63**, 71 (1993).